Cassini RTG Program CDRL Transmittal

TO:
U.S. Department of Energy
Lawrence Livermore Nat'l Lab
7000 East Ave., Bldg. 311 L-293
Attention: Ken Quitoriano

DISTRIBUTION:

Symbol	*Copies*
A	5
B	1
C	1
H	2
J	24
K	1

Cassini RTG Program
Contract No: DE-AC03-91SF18852

In Reply Refer to: **CON #1884**
Date: **20 April 1997**

CDRL Number: **Reporting Requirement 4.F (Document No. RR16)**

Title: **Semi Annual Technical Progress Report (30 September 1996 through 30 March 1997)**
DOE/SF/18852--T75

Approval Requirements:

Approval ☐ None ☒

Contract Period: **11 January 1991 through 30 April 1998**

The technical progress achieved during the period 27 January through 30 September 1996 through 30 March 1997 on Contract DE-AC03-91SF18852 Radioisotope Thermoelectric Generators and Ancillary Activities is described herein.

This report is organized by program task structure.

- 1.X Spacecraft Integration and Liaison
- 2.X Engineering Support
- 3.X Safety
- 4.X Qualified Unicouple Production
- 5.X ETG Fabrication, Assembly, and Test
- 6.X Ground Support Equipment (GSE)
- 7.X RTG Shipping and Launch Support
- 8.X Designs, Reviews, and Mission Applications
- 9.X Project Management, Quality Assurance, Reliability, Contract Changes, CAGO Acquisition (Operating Funds), and CAGO Maintenance and Repair
- H.X CAGO Acquisition (Capital Funds)

Note: Task H.X scope is included in SOW ¶ Task 9.5.
Task H. was created to manage CAGO acquired with capital equipment funding.

Approved: R. J. Hemler, Manager
Space Power Programs

Internal Distribution:
Technical Report List

From: Lockheed Martin Missiles & Space
Room 10B50 Building B
720 Vandenberg Road
King of Prussia, PA 19406

Signature:
Joseph M. Waks
Contracts Manager

LOCKHEED MARTIN

LOCKHEED MARTIN MISSILES & SPACE

Contract No.
DE-AC03-91SF18852

GPHS - RTGs

In Support of the

Cassini RTG Program

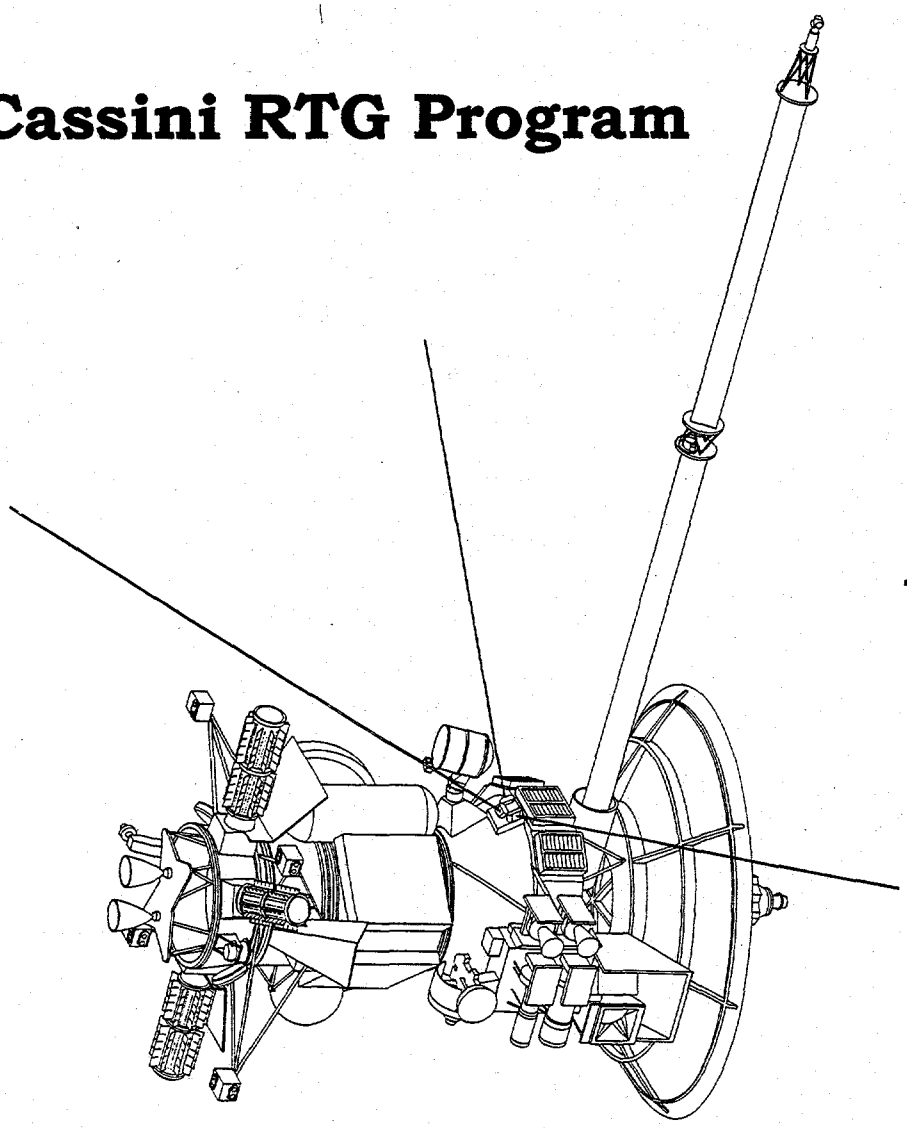

Semi Annual Technical Progress Report

Document No. RR16

30 September 1996
through
30 March 1997

20 April 1997

Space Power Programs

Semi Annual Technical Report

Contract No.
DE-AC03-91SF18852

GPHS-RTGs in Support of the Cassini Mission

Document No. RR16

30 September 1996
through
30 March 1997

Prepared for:

U.S. Department of Energy
Oakland Operations Office
1301 Clay Street
Oakland, CA 94612-5208

Prepared by:

Lockheed Martin Astro Space
P.O. Box 8555
Philadelphia, PA 19101

LOCKHEED MARTIN

Space Power Programs

DISCLAIMER

Semi Annual Technical Progress Report

The technical progress achieved during the period 30 September 1996 through 30 March 1997 on Contract No. DE-AC03-91SF18852, Radioisotope Generators and Ancillary Activities is described herein.

This report is organized by the program task structure as follows:

Table of Contents

List of Illustrations

List of Tables

Table

Task 1

Spacecraft Integration and Liaison

Progress by Major Task

TASK 1 SPACECRAFT INTEGRATION AND LIAISON

Acceptance testing of the RTGs continued during this report period. Magnetics testing of F-7 (October '96) and F-6 (January '97) revealed magnetic fields that differed from those of previous RTGs. Measurements taken during open circuit conditions showed the presence of significant permanent fields in the RTGs. Previously, it had been thought that the RTG magnetic fields were due to uncompensated current loops within the generators. During F-7 magnetic testing possible sources of the anomalous field were investigated and included the gas management valve, electrical connectors and the axial preload spring washers. No significant field sources were found.

Analysis of both the F-7 and F-6 test data by JPL and ESA concluded that the F-7 RTG met the specification limit of 78 nanotesla at a distance of one meter. Their analysis for F-6 showed it to be 80 nanotesla at one meter with an accuracy of ±4 nanotesla. JPL has concluded, however, that the measured F-6 field is acceptable without the use of compensating magnets. Consequently, JPL plans to prepare a wavier for the F-6 magnetic field requirement of 78 nanotesla at one meter. Both the F-7 and F-6 RTGs are acceptable for flight and acceptable magnetic fields can be obtained at the spacecraft magnetometers by properly clocking the RTGs and by assigning a particular RTG to each mounting location. JPL does not plan to use compensating magnets on any of the Cassini RTGs.

Based on thermal vacuum test results and the analysis of gas tap data, power projections have been calculated for the four Cassini RTGs for both beginning of mission (BOM) and 16 years after BOM. Results are shown in Tables 1-1 and 1-2.

Table 1-1. Power Predictions – Beginning of Mission (6 October 1997)

RTG	Power (Watts)		
	Thermal	Electrical Output	Requirement
F-7	4397	298	≥276
F-6	4407	294	≥276
F-2	4378	296	≥274
F-5	4029	251	≥249
F-2, F-6, F-7	13182	888	≥826
F-2, F-5, F-6	12814	841	≥799

Table 1-2. Power Predictions – Power Sixteen Years after BOM (Watts)

RTG	Calculated Electrical Power Output (watts)	Requirement (watts)
F-2	213	≥198
F-6	212	≥199
F-7	215	≥199
F-5	183	≥182
F-2, F-6, F-7	640	≥596
F-2, F-5, F-6	608	≥579

Table 1-1 shows the projected thermal output of the isotope heat source on the planned launch date as well as electrical power output. As can be seen all four RTGs exceed the required output.

Table 1-2 also shows positive power margins for each RTG 16 years after the beginning of mission.

Task 2

Engineering Support

TASK 2 ENGINEERING SUPPORT

RTG Fuel Form, Fueling, and Test Support/Liaison

During this reporting period LMMS continued to provide technical and on-site support for RTG assembly and test operations at Mound. Changes to assembly and test operations manuals were reviewed and approved. Tooling and fixturing P/FRs were reviewed and approved to support assembly operations. LMMS also assisted Mound personnel in preparing documentation for the Buy-off Reviews for both F-2 and F-7. Both RTGs were conditionally accepted by DOE in February 1997.

Specifications and Drawings

Engineering Reports for F-2, F7 and F-6 were issued during this reporting period:

- The F-2 Engineering Report (GESP-7249) was issued as a topical report (CDRL B.2) on 22 November 1996.
- The F-7 Engineering Report (GESP-7250) was issued on 24 January 1997 as a topical report (CDRL B.3).
- The F-6 Engineering Report (GESP-7251) was issued on 7 March 1997 as a topical report (CDRL B.3)

The Final Reliability Assessment Report (GESP-7252) was issued 14 March 1997 as CDRL B.15

An Engineering Report (PIR IVC2-Cassini-146) "Effect of Chugging on Cassini RTGs" was issued on 24 February 1997. This report concluded that chugging of the Cassini Main Engine Assembly (MEA) will not affect performance of the RTGs.

A new Extractor Assembly, Drawing 23021641, was designed for RTG barrel nut removal.

Several ECNs were prepared and processed through CCB in support of the ETG clean-up activities.

Task 3

Safety

TASK 3 SAFETY ANALYSIS TASK

The safety analysis task is comprised of four major activities: 1) Launch Accident Analysis, 2) Reentry Analysis, 3) Consequence and Risk Analysis, and 4) the Safety Test Program. Significant activities performed within each task during this period are detailed in the following subsections.

Table 3-1 is a listing of INSRP meetings held during this reporting period.

Table 3-1. Safety Analysis Task – INSRP Reviews (October 1996 through March 1997)

Date	*Review*
7 January 1997	BEES Subpanel Review of Consequence and Risk Analyses
5-6 February 1997	INSRP Review of Preliminary FSAR Addendum Results
18 March 1997	RESP Preliminary SER Review Meeting

GPHS-RTG Final Safety Analysis (FSAR) Report

Volume 1 (Reference Design Document) and Volume II (Accident Model Document) of the GPHS-RTG FSAR (CDRL C.3) were accepted by DOE and issued 1 November 1996. Volume III (Nuclear Risk Analysis Document) was accepted by DOE and issued 16 November 1996.

The Uncertainty Analysis Document, which is an attachment to Volume III of the FSAR, was accepted by DOE and issued on 24 December 1996. An Executive Summary for the FSAR was also accepted by DOE and issued on that date. This completed issuance of the GPHS-RTG FSAR.

Preliminary results from ongoing analyses for the FSAR Addendum were reviewed with INSRP in February, including the updated source terms resulting from the newly defined Centaur explosion Databook environment and Lockheed Martin's analytical approach for FSII, SRMU coincident impact, SRMU fire effects, and the newly defined phase 0 accident scenarios. Two presentation reports entitled "Phase 0/1 Launch Accident Source Terms" and "Phase 0/1 Launch Accident Consequence and Risk Analysis" were submitted on 28 February and 18 March, respectively, to DOE, NASA, and INSRP.

References cited in the GPHS-RTG FSAR were compiled, with over 90% of the cited references shipped to DOE and INSRP for long term archival.

Launch Accident Analysis

Principal activities in this reporting period have included issuance of LASEP-T (Version 4.0) incorporating updates to the Titan IV/Centaur RTG Databook, generation of new launch accident analysis models for phase 0 and intact launch vehicle ground impacts and completion of accident analyses for the FSAR Addendum.

The effects of Centaur fragment impacts on bare fueled clads and GISs were evaluated for LASEP-T case 1.10 - SV/RTG Impact within Payload Fairing. Representative Centaur fragment characteristics and velocity ranges were defined in order to evaluate the fueled clad damage caused by these fragments using hydrocode analyses. This database was used to update the LASEP-T fragment impact model. The graphite aeroshell failure threshold due to Centaur blast overpressure was also evaluated. Based on the CST-1 data (736±60 psi) which resulted in free flight fueled clads and the CST-8 data (429±40 psi) which retained the fueled clads in graphite, the mean threshold pressure was re-evaluated for the model with the variability and uncertainty range spanning the bounds of the test data. Due to changes in the Databook environment involving the Centaur overpressure, these additional data were not implemented in the most recent version of LASEP-T (Version 4.0).

A detailed assessment of the particle size distributions using the Sandia fireball model was completed. Pre-fireball LASEP-T data were extracted and input into the Sandia code for comparison with the Lockheed Martin fireball model. Using the LASEP-T case 1.1 variability-only run and basing the comparison on mass weighted inhalation effective dose (IED) criterion, the two models agree quite well over the full range of IED values observed.

Full stack intact impact (FSII) model development was completed per the environment definition specified in Revision A of the Databook. The FSII accident simulation model was updated to include a 3-dimensional trajectory simulation similar to that used for the SRMU fallback probability calculation. This approach determines the probability of coincident impact of RTG components and SRMU fragments for nose-first, launch vehicle intact impacts. Due to time constraints imposed by the recent Databook updates, the FSII model was not included in LASEP-T Version 4.0. A standalone version of LASEP-T was

developed for FSII simulations. SRMU coincident impact and SRMU fire effects were included directly in the FSII model.

LASEP-T was modified to extract additional data on GPHS module and fueled clad spatial distributions for use in the SRMU propellant fallback modeling. Information on module and space vehicle initial velocities was also extracted as modeling input. Additional LASEP-T runs were performed to include information needed for the SRMU fallback analyses. Data specific to the SRMU probability calculations were generated.

With the new version of LASEP-T, modifications to the post-processing routines were required. These routines provided such information as type of surface impacted, type of insult to RTG, percentiles of the releases, etc. These additions led to a significant rewrite of the post-processing programs.

Case 1.10 model development has been completed and code checkout was performed. The process of incorporating case 1.10 into Version 4.0 of LASEP-T was completed.

Centaur overpressure values defined in Revision A of the Databook were revised in a Revision B change proposal to reflect new data from a series of joint NASA/NASDA safety tests. These modifications which reduced the mean static overpressure from 120 to 39 psi, required substantial changes to the current 4.0 version of LASEP-T. The overpressure environment was incorporated into LASEP-T and code checkout was completed.

Probability calculations for intact modules and space vehicles have been completed using the revised Centaur overpressure. The probability calculations to assess aft segment impact coincident probabilities were also performed.

The sequence of events during phase 0 (pre-launch) accidents has been redefined in a Databook Revision B change proposal. These late changes have impacted the method in which phase 0 accidents can be analyzed. In order to obtain timely results, it was decided to code phase 0 separately from LASEP-T, extracting the necessary models to maintain a consistent set of assumptions for the analyses. The methodology applied to the phase 0 accident scenarios is somewhat different due to the various environments that can occur during the pre-launch phase. Phase 0 model development and checkout has been completed.

LASEP-T cases 1.1 through 1.10 were analyzed using the recently updated Centaur overpressure environment. Case 1.10, which was not included in the previous FSAR analysis, had little impact on the total source term distribution for phase 1.

Integration of LASEP-T source terms for cases 1.1, 1.3 and 1.10 with the SRMU coincident fallback source terms was completed. The integrated source terms were submitted for consequence calculations. The probability of solid propellant fragments hitting multiple modules was factored into the consequence analysis for these cases.

SRMU Fallback and Fire

The SRMU fallback environment applies to accident scenarios in which an SRMU propellant fragment or entire segment lands on top of, or sufficiently close to an RTG or RTG component to present a threat to the containment of plutonia fuel. The SRMU propellant fragments are presumed to be ignited, and so there is also a solid propellant fire environment, which may subject RTG components to a high temperature combustion zone for periods of a few hundred seconds. During the current reporting period, these environments have been modeled to determine the conditional probability of occurrence and magnitude of potential source terms arising from them.

Fallback and Fire Conditional Probability

The conditional probability modeling produces tabulated probabilities for the coincident impact of SRMU fragments onto modules resting on sand and concrete, with the time constraint that the RTG component lands first, and for the adjacent impact on the same surfaces without the time constraint. The former provides the conditional probability that the fallback environment applies, and the latter that the fire environment applies. Probability density was summed over discrete ranges of SRMU propellant fragment characteristics, comprising 16 mass bins and 12 velocity bins. It was assumed that the fragment drag coefficient, c_d = 0.5, and that accidents occurring at altitudes greater than 1737 meters (5700 ft) are assumed to be of negligible probability and significantly less likely to generate source terms because of the increased likelihood of water impact. The joint probability of two SRMU fragments or segments impacting modules or a spacecraft in the same trial was also assumed to be negligible. Correlation of SRMU-induced releases and non-SRMU-induced releases was assumed to be negligible.

For a particular launch vehicle position, velocity, and orientation, the probability that a single module on the spacecraft impacts the ground proximal to an SRMU propellant fragment is given by a seven-fold integral subject to the condition that

$$D^2 \geq (x_m - x_f)^2 + (y_m - y_f)^2 \qquad [3\text{-}1]$$

where D is a characteristic distance and x and y refer to locations in the ground coordinate frame. This is further constrained for the direct impact condition, by insisting that the module lands before fragment impact. By employing the Jacobian of the transformation relations, the probabilities can be evaluated numerically.

These calculations were performed for a subset of trials from cases 1.1, 1.3, and 1.10. The first 500 LASEP-T trials in each case were analyzed, excluding any over the 5700 ft. threshold. Both the probability of free module impact, and space vehicle impact were calculated and then adjusted for the expected number of modules associated with each of these conditions as given in Table 3-2.

Table 3.2. Summary of Expectation of Probability of Coincident Impact

Case	*Module on Sand*	*Module on Concrete*	*SV on Sand*	*SV on Concrete*
1.1	5.914×10^{-8}	7.224×10^{-8}	1.442×10^{-7}	5.903×10^{-7}
1.3	3.723×10^{-10}	4.623×10^{-9}	1.139×10^{-8}	1.769×10^{-7}
1.10	2.184×10^{-10}	3.589×10^{-9}	1.539×10^{-9}	2.133×10^{-8}

These probabilities were further adjusted to account for the actual spatial distribution of modules about the SV debris centroid, and for the possibility that an SRMU fragment impacts multiple isolated modules in a single impact event. Both of these can be accounted for by analysis of the actual module distribution associated with the specific trial results from LASEP-T.

The results for conditional probability given above were calculated for single modules or a single space vehicle. All four probability calculations were performed for each LASEP-T trial under consideration, although the values stated above are aggregated over all trials analyzed. To determine appropriate weighting factors for a given trial, it was necessary to examine the distribution of RTG components on the ground for each trial. From this

examination, the number of modules, n, which remained with the space vehicle, and the number which were released at altitude, (54-n), were determined as well as partitioning these according to sand and concrete surface impacts.

There remains the possibility that a single SRMU fragment may impinge on multiple GPHS modules. For each trial, the launch pad coordinates of each of the GPHS modules was the subject of a frequency analysis to determine the likelihood that a single SRMU propellant fragment will impact more than one of the modules.

Representing the fragment impact area as a disk, each of the module locations was "masked" by this disk in turn. By listing and sorting all discrete coordinate indices on a common basis, the fragment positions yielding multiple module impacts were identified. The relative frequencies, normalized to the total count, provided a reasonable estimate of the probability of multi-module impact.

Fallback Response

To evaluate the response to the fallback environment, calculations employing coupled Eulerian-Lagrangian code PISCES-2DELK, referred to as hydrocode, were performed by Orbital Sciences Corporation with the assistance of Foils Engineering. An initial concern that fragment impact would result in explosive burning, was shown to be unwarranted, as damage sustained by an RTG component results almost entirely from the mechanical insult, with less than a 2% difference in distortion if the overpressure insult is included in the model. A distortion model was constructed using the hydrocode results, yielding distortion predictions for impact on concrete and impact on sand, including variability in fuel mechanical properties, represented by weak and strong fuel properties. To determine if the distortion resulted in a source term, the distortion-to-release model employed in LASEP-T was extended to include the larger distortions possible with SRMU fragment impact. The probability of breach used in this analysis was

$$P_{breach}(d) = 1 - e^{-5.66(d-0.13)} \qquad [3\text{-}2]$$

The breach regimes modeled were extended to include an extrapolated regime for large distortions. The boundary threshold between the small and large release regimes used in LASEP-T simulations was randomly selected from a normal distribution characterized by a

mean, μ=0.477 and standard deviation, σ=0.053. Similarly, the boundary between large and extrapolated regimes was also selected randomly, with μ=0.715 and σ=0.06, based on the largest distortion value in the test database.

To determine source terms where a breach was predicted using Equation [3-2], a random number was drawn from a uniform distribution and was compared to threshold values obtained from the selected boundary thresholds. If less than the lower threshold, the release was taken to be in the small regime. If the drawn value is larger than the lower threshold, but less than or equal to the larger threshold, the release was taken to be in the large regime. If larger still, the release was taken to be in the extrapolated regime. The overall breach probability, and the individual regime threshold probabilities are shown in Figure 3-1 as a function of distortion.

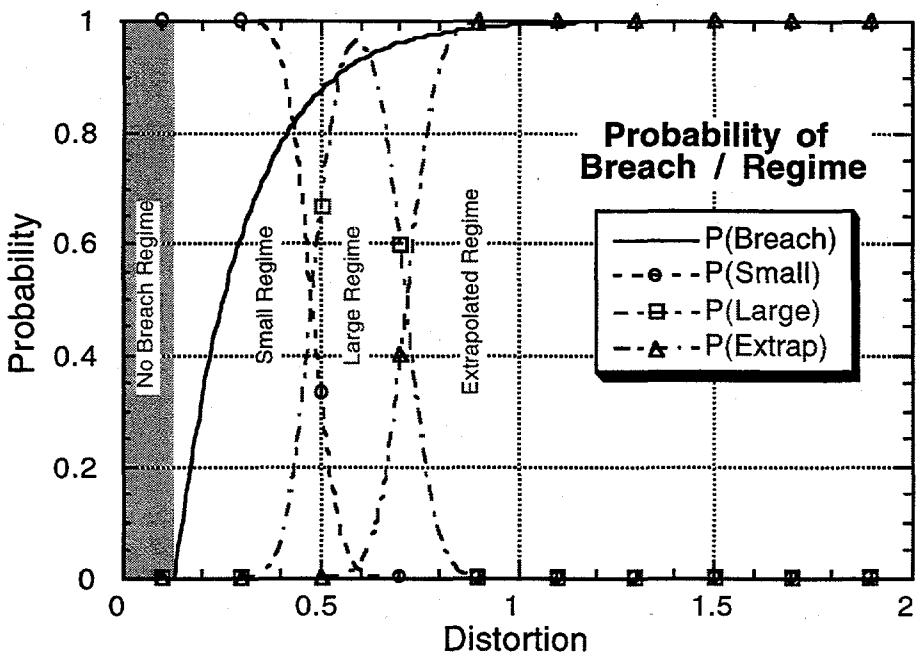

Figure 3-1. Probability of Breach (Solid Line) and Breach Regime Threshold (Dashed Lines)

Depending on the regime, the existing LASEP-T model was used to determine the fractional release. For distortions, $\delta > 0.4677$, when an extrapolated regime was indicated, the fractional release was determined as $f = 0.4372 (d - 0.4677)$.

Solid Propellant Fire Response

The response model for a solid propellant fire is based on experimental evidence, thermal analyses, and extensions of the vaporization, condensation, and agglomeration models present in LASEP-T. The SRMU fallback environment includes the probability that an RTG component already on the ground would be struck by a falling propellant fragment resulting in possible release. For all phase 1 accidents, for which SRMU fallback and fire environments are potentially applicable, the fragments were assumed ignited prior to impact. The SRMU solid propellant fire environment was also applied in determining the final particle size distribution of the additional release.

The response of intact RTG components to the SRMU propellant fire was based on experimental data in which components survived a fire using a similar propellant, and these results were confirmed for the current propellant material using a computer-aided thermal analysis employing the SINDA computer code. The response of any released material in the presence of an SRMU propellant fire was determined by analysis of the vaporization and agglomeration effects for the fire description given in the Databook, and is similar to the model employed in the FSAR work for liquid propellant fires.

Tests performed by Los Alamos[1] showed no containment failures for bare fueled clads placed adjacent to burning solid propellant fuel. These results, in conjunction with a computer aided thermal analysis, support the conclusion that the response model need not include the possibility that the SRMU propellant fire environment could induce releases in otherwise unbreached RTG components. In order to confirm that these test results could be extended to the SRMU solid propellant environment, a thermal calculation was performed using a computer numerical code and the results were verified by hand calculation of bounding cases.

Thermal analysis of the SRMU solid propellant fire environment was conducted in order to determine the response of a bare clad. A nominal heat flux value of 837.36 kJ/m^2-sec

[1] Pavone, D. and C. Seabourn, "Solid Propellant Fire Test," writing in "Space Nuclear Safety Program Progress Report," LA-9934-PR for June 1983, edited by S.E. Bronisz, and issued (Nov 1983).

(20 cal/cm^2–sec), and directional values of ±40% of nominal, were used based on Sections 12.7.3.2 and 12.7.3.1 of the Databook. This analysis was extended to consider a clad subject to fires from multiple sources, such that all surfaces are exposed to the maximum flux of 1172.3 kJ/m^2-sec or 1.4 times the nominal flux, for periods of up to 600 sec (10 min). Even in this extreme circumstance, the Ir clad will not melt, based on the expected post-exposure emissivity of the clad of 0.8. The maximum clad temperature was determined to be 2201K (1928°C) which is well below the Ir melting temperature of 2727K (2454°C).

These analyses lead to the conclusion that an intact bare Ir clad will survive a solid propellant fire, as long as the emissivity is increased by exposure to the fire. Moreover, the thermal margin improves dramatically if the clad remains within an intact GIS or GPHS module as these are also expected to survive the fire, based on LANL tests, and significantly increase the thermal mass protecting the clad.

Since intact GPHS modules, and even bare clads, survive maximum exposure to the solid propellant fire, the effect of this environment is to modify the particle size distribution of releases that occur due to other insults but are subsequently subject to this environment, resulting in vaporization followed by condensation and agglomeration.

The same vaporization model used in LASEP-T was adapted to the conditions given for the solid propellant fire environment. Two cases were considered: vaporization of particles at a fixed point in the combustion zone and vaporization of particles entrained in the combustion flow field.

The vaporized fuel was assumed to condense heterogeneously and agglomerate with alumina - one of the primary combustion products of the propellant fire. The amount of alumina available for agglomeration was taken to be the amount developed during the average length of time required to expose an impacted RTG component for a propellant fragment of a given size.

The initial particle size assumed for the condensate material is 30Å, based on the analysis of Sokolowski, et al.[2]. The alumina condenses as γ-Al_2O_3 with a density of approximately 3.2 g/cm^3. The agglomeration model employed Smoluchowski's solution in a

[2] Sokolowski, Sokolowska, Michalski, and Gokieli, *J. Aerosol Sci.* 8 p.219 (1977).

simplification of the VANESSA model, as was used in LASEP-T. The resulting particle size distribution is shown in Figure 3-2.

To determine the density of the distributed vapor, the amount of alumina available for heterogeneous condensation and agglomeration was assumed to be related to the amount of time required for the fragment to burn-back far enough to reveal the RTG component underneath. Based on the ratio of the density of alumina in the fire effluent to that of the effluent gas, the alumina product accounts for about 28% of the mass consumed by combustion.

The propellant fragment was assumed to be a right-circular cylinder with a cross-sectional area with an aspect ratio (height:diameter) of 1:1, unless this yielded a height exceeding the web thickness. The circular face was assumed to be covering the RTG component. For a module located at a random position under the fragment, the expected value of the burn-back time is obtained by integration. For three values of web thickness appropriate to the various cases analyzed, specifically 38, 17, and 11 inches, the corresponding expectation values are presented in Figure 3-3.

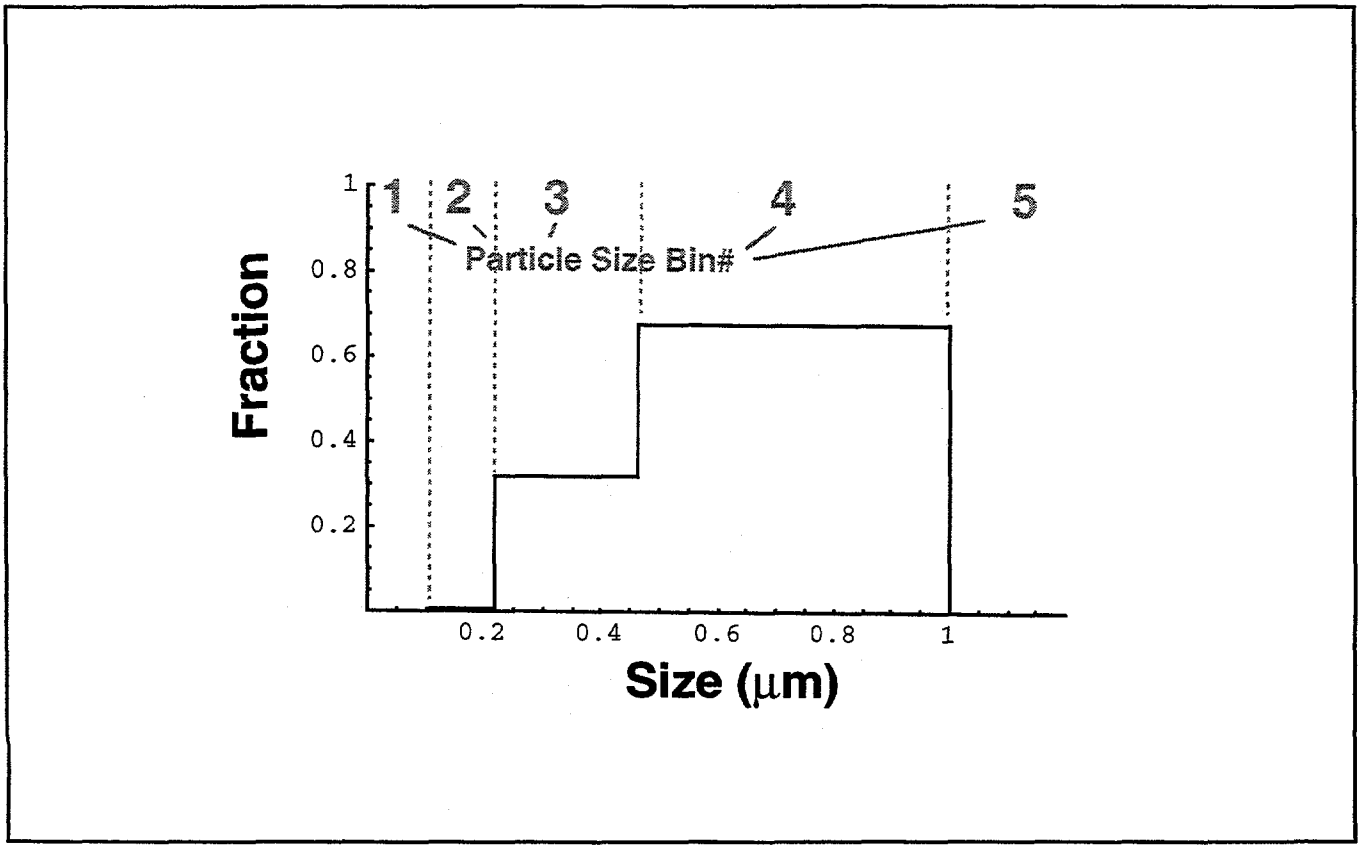

Figure 3.2. Particle Size Distribution for Vapor Resulting from SRMU Propellant Fires

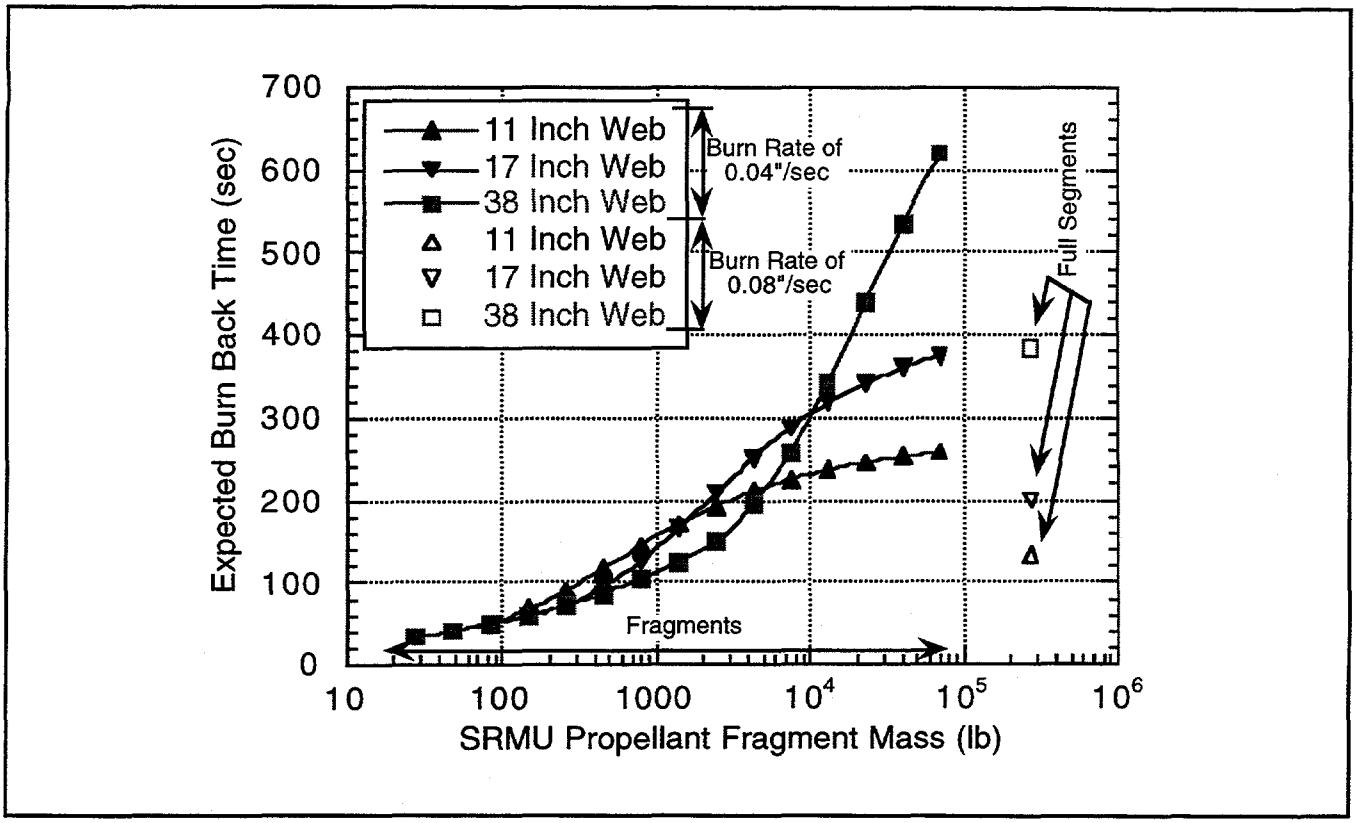

Figure 3-3. Expected Burn-Back Times for SRMU Fragments and Segments

The fire environment effects were applied to the source terms calculated for the SRMU fallback environment, with the offset taken to be zero for the expected burn-back time, then with the offset varying as the particles become entrained in the combustion flow. These two conditions were modeled using the table driven BINSWTCH code that is part of LASEP-T. Two data tables were used, one which models the effect of the fire when the propellant fragment is on top of the module, and the other which models the effect of the fire once the fragment has burned away to the point of exposing the impacted module.

Vapor developed by the application of the fire environment was distributed using the SDSTVAP subroutine which redistributes the quantity of fuel vaporized into particle size bins as shown in Figure 3-2. Burn-back time was also used to calculate the amount of alumina available for agglomeration. The agglomeration process required adjustment of the source term density. In all cases analyzed, the agglomerated material contained a very small mass fraction of plutonia, thus the density of the agglomerated material is essentially that of γ-alumina, 3.2 g/cm^3.

The fallback response model to determine source terms due to SRMU propellant impact was combined with the fire model to determine the effect on these source terms, arriving at final source terms for cases involving SRMU propellant fallback and fire. The source term results were combined with conditional probability results, and tabulated for consequence and risk analysis. Fire effects on source terms arising from unrelated causes, such as impact of modules on concrete, were not computed.

Uncertainty Analyses

In the last six months, our "deconvolution" method for performing uncertainty analyses was finalized and implemented for the Cassini launch safety analysis. Procedures for performing sensitivity analyses to determine the contribution of individual model parameters to overall uncertainty were also implemented.

The deconvolution procedure used for the Cassini safety analyses was more general than the originally proposed procedure, which was based on the assumption that the variability-only consequence, the variability-plus-uncertainty consequence, and the uncertainty multiplier determined by deconvolution are all distributed according to the lognormal distribution. This was found to be a poor assumption for launch accident consequences and consequences arising from inadvertent reentry during the Earth Gravity Assist Swingby. The only assumption in the implemented procedure is that the uncertainty multiplier is distributed according to the lognormal distribution. Consistency tests showed this to be a good approximation with standard errors for the parameters of the uncertainty multiplier of about 0.03 orders of magnitude.

The procedure for determining the contributions of individual parameters to overall uncertainty involves performing a step-wise regression analysis of the variability-plus-uncertainty consequence for the individual parameters and weighting the regression coefficients by the standard deviations of the parameter distributions.

Also, The LASEP-T code was modified to enable generation of an additional output file which contains the parameter values used in each trial for variability-plus-uncertainty calculations. This new file enables the determination of the sensitivities of the fuel source terms to the values of the parameters.

Reentry Analyses

GIS Steep Trajectory (2-D Cylindrical CFD): Coupled RACER (flowfield)/LORAN-C (radiation) solutions were obtained for selected points on the steep trajectory for the GIS following the predicted failure of the GPHS aeroshell. The RACER/LORAN-C codes, originally formulated for axisymmetric flow, were extended to treat the cylindrical GIS geometry. Following the approach used for analysis of the GPHS aeroshell, at each of the GIS trajectory points, coupled RACER/LORAN-C solutions were generated for three specified wall temperatures. A matrix of ablation rates and net heat flux, as a function of wall temperature and altitude, was then constructed. The REKAP in-depth transient-heating code was modified to interpolate these tables and compute the GIS temperature and recession history. In REKAP, the surface temperature is determined by iterative solution of the surface energy balance equation. Recession is obtained by integrating the ablation rate.

Figure 3-4 shows the surface temperature history immediately following a postulated release at 1.9 seconds. The REKAP solution, previously obtained by using correlations for heating and ablation rates (rather than the more rigorous RACER/LORAN-C computational fluid dynamics (CFD) approach), is compared in Figure 3-4 with the new CFD-REKAP technique. As expected, based on similar comparisons for the GPHS aeroshell, the use of heat-flux correlations leads to an over-prediction of surface temperature.

Figure 3-5 compares the predicted surface recession for REKAP with and without CFD. Again, the use of approximate correlations leads to an over-prediction. At 2.4 seconds, the use of CFD results in a 40% reduction in surface recession.

The REKAP/CFD in-depth temperature profile at 2.4 seconds is shown in Figure 3-6. The iridium clad/FWPF boundary has almost reached the iridium/FWPF eutectic temperature of 4625°R. The iridium has not yet started to melt (4909°R) and the fuel is still below its melt temperature (4812°R).

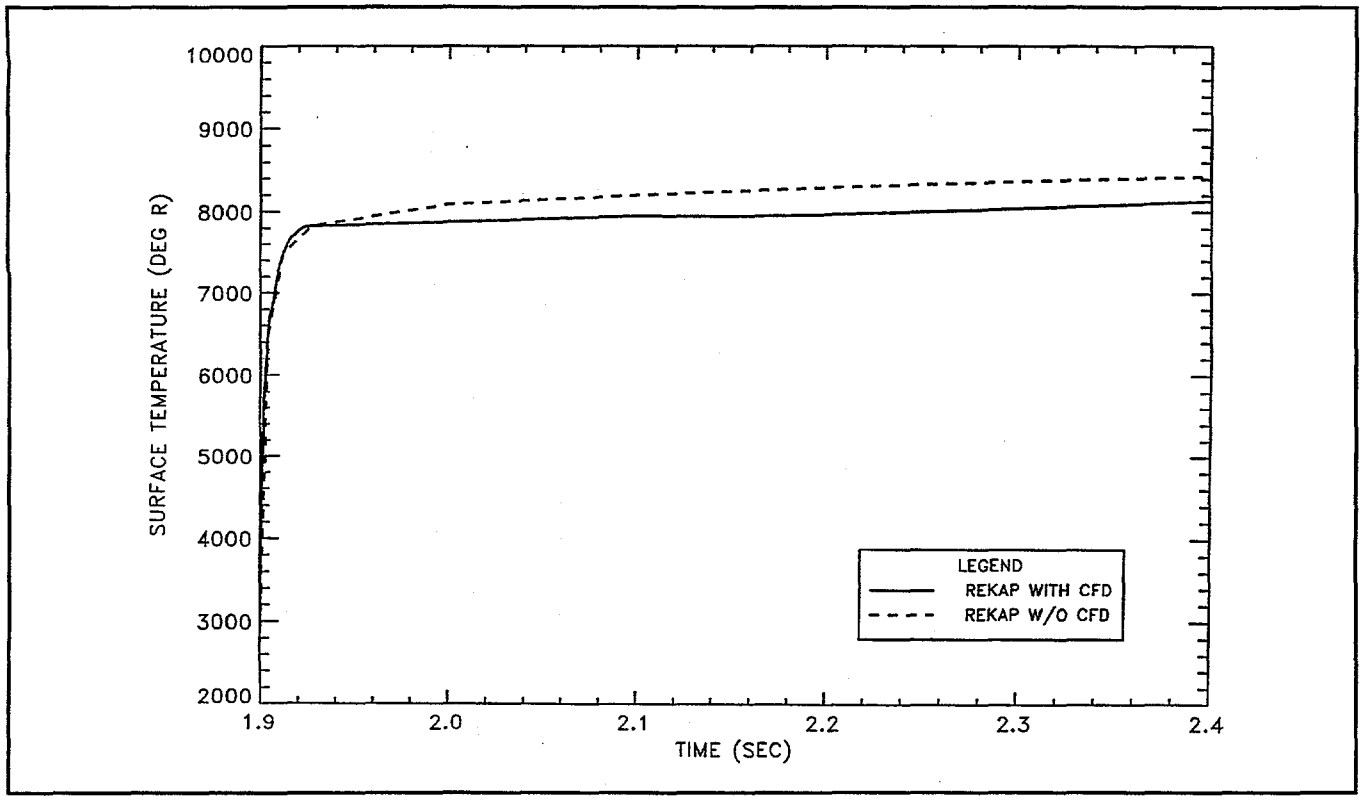

Figure 3-4. GIS Surface Temperature History Immediately Following Release along the Steep Trajectory. Comparison of REKAP Solutions Based on Correlations with REKAP Using CFD

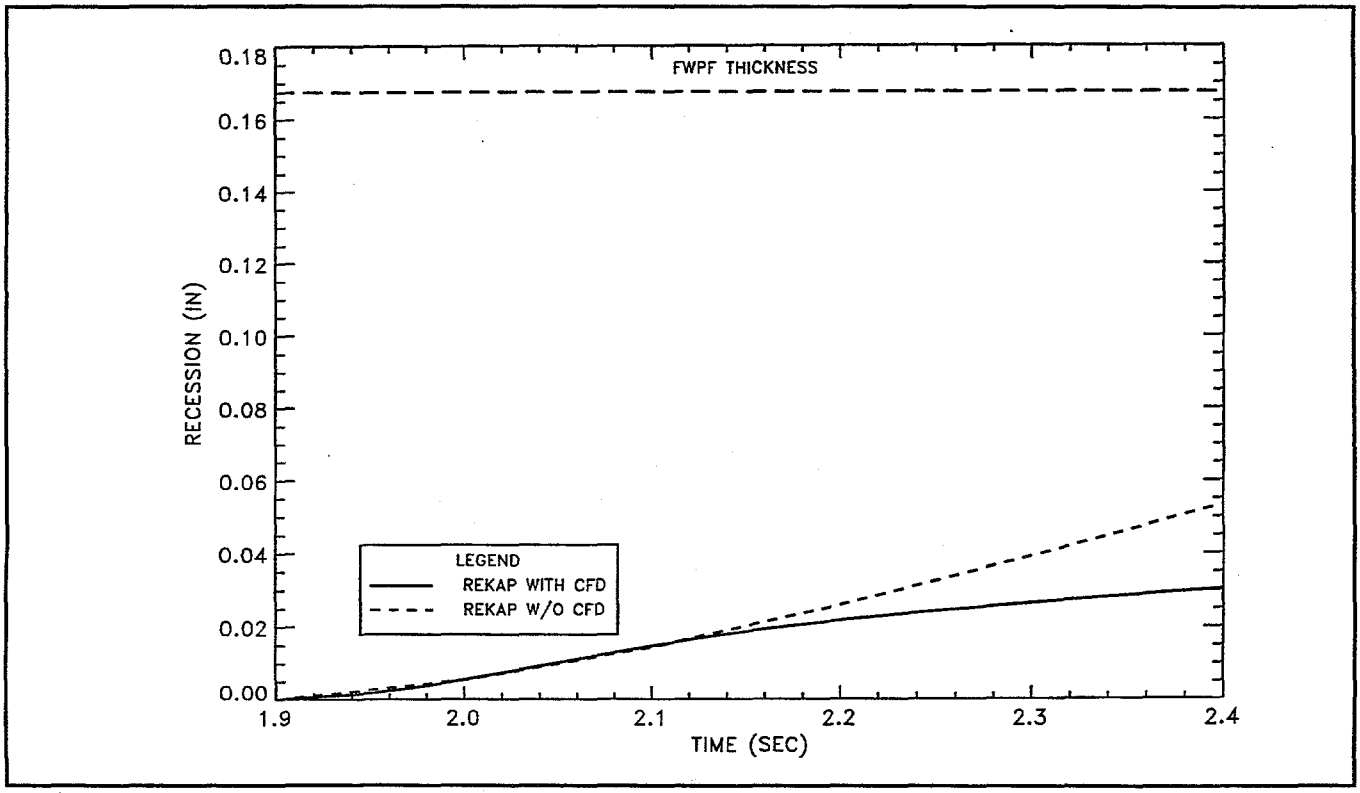

Figure 3-5. GIS Recession History Immediately Following Release along the Steep Trajectory. Comparison of REKAP Solutions Based on Correlations with REKAP Using CFD

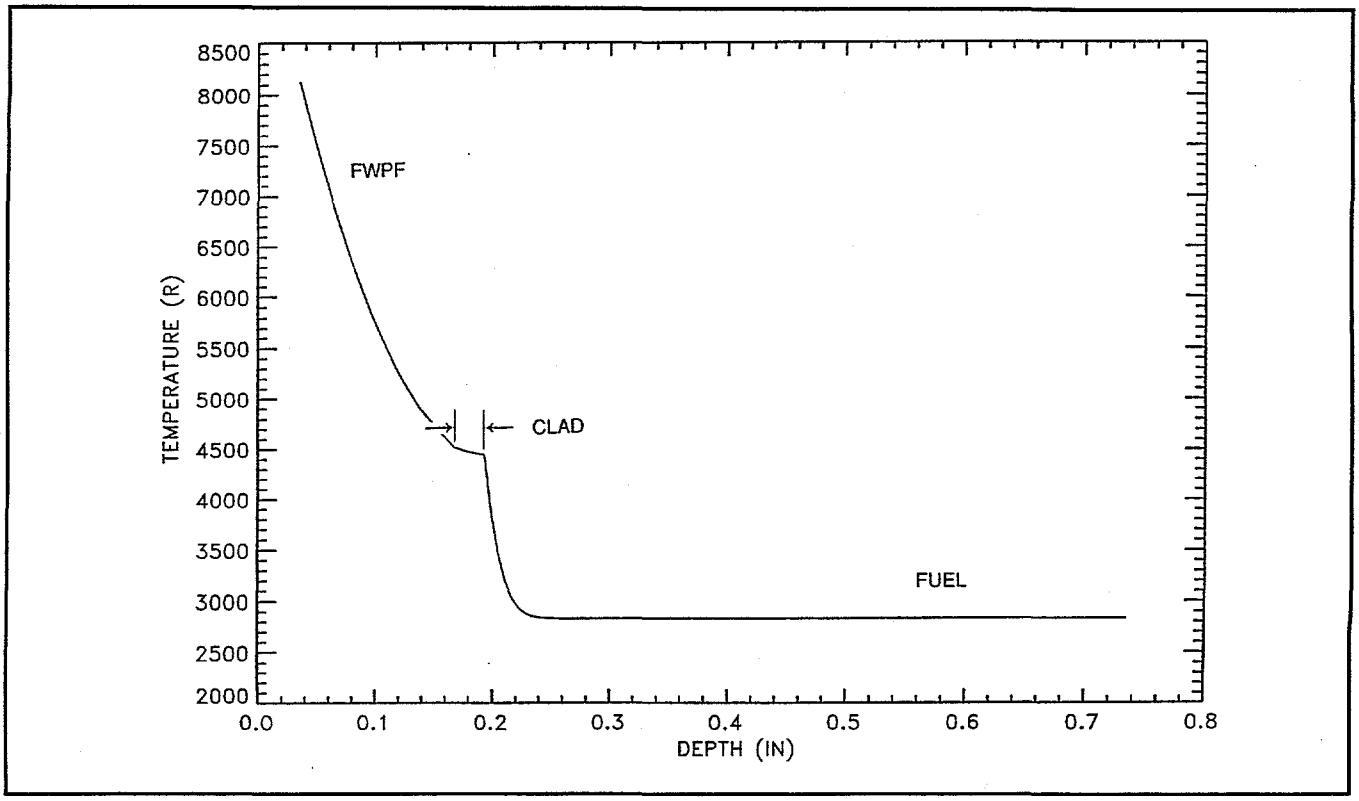

Figure 3-6. GIS In-Depth Temperature at 2.4 Seconds (0.5 Seconds Following Release) along the Steep Trajectory

Stagnation-Line Version of RACER/LORAN-C: The RACER and LORAN-C codes compute the flowfield and radiative heating on the entire front face of the GIS (oriented broad-side to the flow). However, only the stagnation point results are used in the one-dimensional, transient, in-depth thermal response code (REKAP). In addition, the cylindrical shape of the GIS permits the use of a separate stagnation-line flow solver. Therefore, to greatly reduce the run time of RACER and LORAN-C for the GIS, and maintain consistency with the stagnation-point REKAP approach, a modification to RACER was developed to solve the flow only along the cylindrical stagnation line. The development of this version of RACER will greatly expedite solution of the remainder of the steep and the intermediate ($\gamma = -20^{\circ}$) trajectories.

The 2-D/axisymmetric full Navier-Stokes (FNS) equations governing the hypersonic flow over a cylindrical/spherical stagnation point region can be written in the following form

$$\mathbf{f}_{1,\xi_1} + \mathbf{f}_{2,\xi_2} = \varepsilon(\mathbf{s}_{1,\xi_1} + \mathbf{s}_{2,\xi_2}) + \mathbf{h} \qquad [3\text{-}3]$$

where

$$\mathbf{h} = [0,0,0, -j\,p/Jz, (\gamma_\infty p - Z^* \rho T)]^T \qquad [3\text{-}4]$$

and $j = 0$ for 2-D flows and $j = 1$ for axisymmetric flows. These six equations include the five differential conservation of mass, momentum and energy, and the sixth equation is the equation of state for the gas mixture.

For 2-D as well as axisymmetric flows, the streamwise viscous effects along the stagnation streamline are negligible due to flowfield symmetry effects; i.e., $\mathbf{s}_{1,\xi_1} = 0$ at $\xi_1 = 0$. Thus, for such cases the governing FNS equations along the stagnation streamline become

$$\mathbf{f}_{1,\xi_1} + \mathbf{f}_{2,\xi_2} = \varepsilon \mathbf{s}_{2\xi_2} + \mathbf{h} \quad \text{along } \xi_1 = 0 \qquad [3\text{-}5]$$

where the first five equations are the differential conservation equations and the sixth equation is the algebraic equation of state.

These governing flowfield equations vanish along the stagnation streamline (at $\xi_1 = 0$), thus, the flowfield solution is singular. Furthermore, the transformed governing equations are divided by the transformation Jacobian (J) which also vanishes along the stagnation streamline. However, all singularities can be removed by expanding the flowfield and coordinate metrics around the stagnation streamline and then taking the limit $\xi_1 \to 0$, where the ξ_1 coordinate starts at the stagnation point and is measured along the cylindrical/axisymmetric body surface.

Expanding the flowfield variables, using the following Taylor series expansions which include the odd/even behavior of the flowfield quantities with respect to the stagnation streamline, yields

$$\rho(\xi_1,\xi_2) = [\rho_1(\xi_2)] + [\rho_2(\xi_2)]\,\xi_1^2 + O(\xi_1^4) \qquad [3\text{-}6]$$

$$u(\xi_1,\xi_2) = [u_1(\xi_2)]\,\xi_1 + [u_2(\xi_2)]\,\xi_1^3 + O(\xi_1^5) \qquad [3\text{-}7]$$

$$v(\xi_1,\xi_2) = [v_1(\xi_2)] + [v_2(\xi_2)]\,\xi_1^2 + O(\xi_1^4) \qquad [3\text{-}8]$$

$$p(\xi_1,\xi_2) = [p_1(\xi_2)] + [p_2(\xi_2)]\,\xi_1^2 + O(\xi_1^4) \qquad [3\text{-}9]$$

$$T(\xi_1,\xi_2) = [T_1(\xi_2)] + [T_2(\xi_2)]\,\xi_1^2 + O(\xi_1^4) \qquad [3\text{-}10]$$

In this flowfield expansion the subscript 1 refers to first-order terms and the subscript 2 refers to the second-order term in the expansion. In all there are five first-order terms and five second-order terms (ten unknowns in all). By considering the behavior of the flowfield variables in the freestream at ξ_2 = LMAX, and along the body at ξ_2=1, the following approximations for v_2, u_2, ρ_2 and T_2 satisfy the freestream and wall boundary conditions.

$$v_2(\xi_2) = -v_1(\xi_2)/2\ ,\ u_2(\xi_2) = v_1(\xi_2)/6,\ \rho_2(\xi_2) = T_2(\xi_2) = 0 \qquad [3\text{-}11]$$

Thus, out of the ten flowfield unknowns (ρ_1, v_1, u_1, T_1, p_1, ρ_2, v_2, u_2, T_2 and p_2), approximate distributions determine four (v_2, u_2, ρ_2 and T_2) and the remaining six (ρ_1, v_1, u_1, T_1, p_1 and p_2) are solved using the governing flowfield equations. Similar expansions can be obtained for the transformation Jacobian (J) and the transformation metrics.

$$J = [J_1(\xi_2)] / \xi_1 + [J_2(\xi_2)]\,\xi_1 + O(\xi_1^3) \qquad [3\text{-}12]$$

$$\xi_{1,x}/J = [a_{1x1}(\xi_2)]\,\xi_1^2 + [a_{1x2}(\xi_2)]\,\xi_1^4 + O(\xi_1^6) \quad \text{etc.} \qquad [3\text{-}13]$$

For simplicity, only the expansion for $\xi_{1,x}$ is shown here; however, similar expansions can be obtained for the remaining eight transformation metrics. Unlike the flowfield expansions shown earlier, all the first-order and second-order terms appearing in the Jacobian and metric expansions can be analytically obtained from a knowledge of the coordinate transformation used.

After substituting these expansions for the flowfield and coordinate metrics into the five governing equations representing the conservation of mass, momentum and energy, and the equation of state, the governing equations in the vectorial form become,

$$[\mathbf{f}_0 + \mathbf{f}^{\pm}_{2,\xi_2} - \varepsilon\mathbf{s}_{2,\xi_2} - \mathbf{h}]\xi_1 + [\text{Second-Order Equations}]\,\xi_1^2 + O(\xi_1^3) = 0 \qquad [3\text{-}14]$$

For these governing equations to be valid independent of ξ_1, all coefficients of this vectorial equation must be zero. In all, five first-order equations and five second-order equations (a total of ten governing equations) are available for the ten flowfield unknowns (ρ_1, v_1, u_1, T_1, p_1, ρ_2, v_2, u_2, T_2 and p_2). However, a review of these equations shows that the only second-order term appearing in the five first-order equations is p_2. This clearly shows that the

remaining second-order terms (ρ_2, v_2, u_2 and T_2) are indeed not very important, and the approximate flowfield expansions mentioned earlier are adequate for them, since they satisfy the important freestream and wall boundary conditions. To solve for the remaining six flowfield unknowns, five first-order equations and one second-order equation (corresponding to the z-momentum equation) are chosen. These six equations are then solved for the six unknowns

$$\mathbf{q}_{stag} = [\rho_1, \rho_1 u_1, \rho_1 v_1, T_1, p_1, p_2]^T \qquad [3\text{-}15]$$

The five first-order equations are solved using flux-vector splitting, and the second-order equation is solved using central differencing. The overall solution is done using an iterative algorithm based on a linearization of the governing equations around the previous iteration. This results in fully-implicit block-tridiagonal system of equations, which is solved using boundary conditions at the body and the outer freestream boundary.

The new cylindrical stagnation-line only version of RACER has been validated by comparisons with the existing cylindrical RACER code (the cylindrical RACER code had previously been validated by comparisons to experimental data as well as other numerical techniques). The predicted stagnation-streamline pressure profile from the two versions of RACER is shown in Figure 3-7. The corresponding temperature profile comparison is shown in Figure 3-8. Agreement between the two codes is excellent. As expected, the stagnation-line only version runs over twenty-times faster than the cylindrical version of RACER. LORAN-C for the stagnation line also runs proportionally faster.

Surface Energy Balance: The SEB is the vital link between the flowfield environment and the thermal response of the module. The temperature and ablation history of the GPHS module and the GIS are computed using in-depth, transient-heating codes. Module and GIS temperature and recession are driven by the heat flux reaching the surface. This heat flux, due to the chemically reacting, radiating, shock-layer gases, and the mass transfer of ablation products, is communicated to the surface through the SEB equation. The SEB equation expresses the conservation of energy at the surface boundary. The net heat flux to the solid surface results from summing gas-phase conduction, diffusion and radiation, and energy transfer due to mass removal, heterogeneous reactions, and re-radiation from the surface to the surrounding gas.

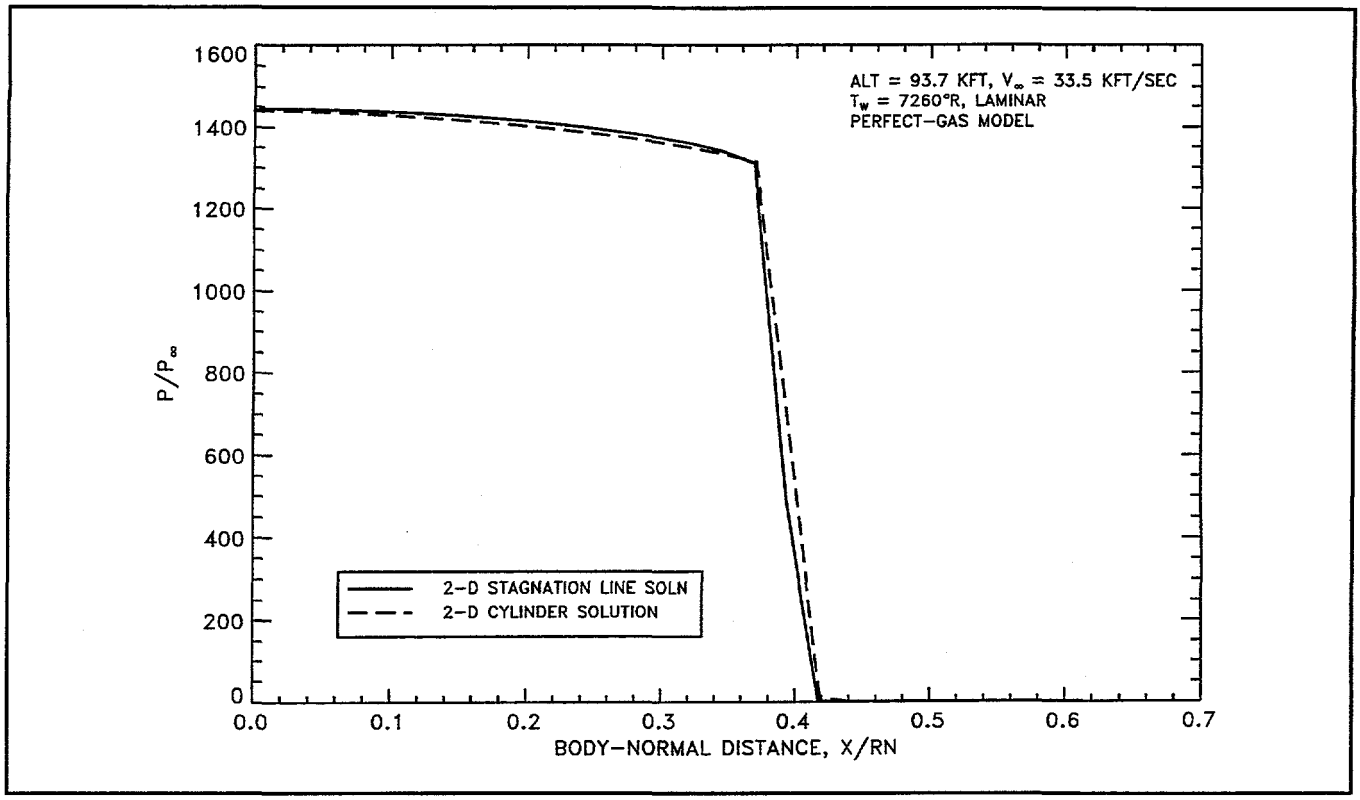

Figure 3-7. Comparison of the Stagnation-Streamline and 2-D Cylindrical Versions of RACER. Pressure Profile along the GIS Stagnation Streamline

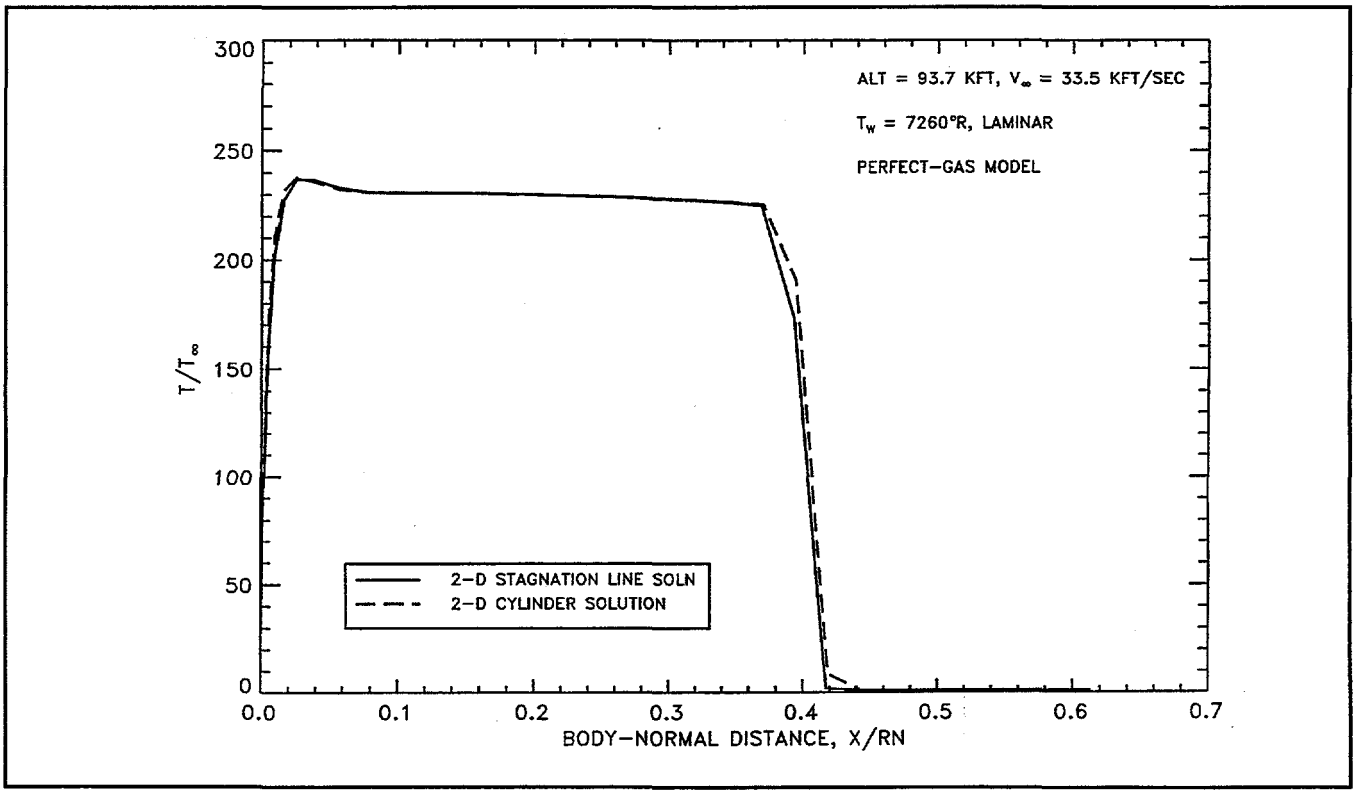

Figure 3-8. Comparison of the Stagnation-Streamline and 2-D Cylindrical Versions of RACER. Temperature Profile along the GIS Stagnation Streamline

Lockheed Martin Missiles & Space (LMMS) and the Interagency Nuclear Safety Review Panel/Reentry Sub-Panel (INSRP/RESP), advocate different formulations for the SEB at an ablating carbon surface. The LMMS form has been used in all Earth gravity assist (EGA) accidental reentry computations documented in the Cassini FSAR. Several attempts have been made to resolve the differences in the SEB, including various derivations and the analysis of simple model problems. In addition, LMMS sought an independent assessment of this issue. Despite these efforts, a mutually acceptable form for the SEB has not been obtained. In order to quantify the differences in the SEB formulations, a new set of computations for the steep EGA trajectory has been performed.

LMMS SEB Formulation: LMMS and its subcontractor, AeroTechnologies, Inc., have formulated and employed an SEB that incorporates nonequilibrium sublimation and oxidation of the carbon surface. The nonequilibrium ablation model, and the heterogeneous oxidation model, provide the mass flux of each species being injected into the shock layer.

Since the catalytic nature of the surface is not known, a worst-case (for heating) equilibrium-catalytic boundary is assumed. In this model the ablation products instantaneously react with the shock-layer gases and form an equilibrium mixture at the wall.

The LMMS form of the SEB differs in only one term from that employed in conventional ablation codes. In the LMMS approach the net heat released due to sublimation and oxidation of carbon is given by:

$$-\left(\sum_{i=1} \dot{m}_i^{inj} h_i - \dot{m}_w h_s\right) \qquad [3\text{-}16]$$

but in the conventional approach this is replaced by:

$$-\left(\dot{m}_w h_w - \dot{m}_w h_s\right) \qquad [3\text{-}17]$$

In the LMMS approach the flowfield is computed at a specified wall temperature. The LMMS SEB formulation distributes the energy of the homogeneous gas-phase reactions (forming the equilibrium mixture) into heating the surrounding gas.

INSRP/RESP Approach: INSRP/RESP, in an evolving sequence of technical notes, came to the conclusion that the LMMS form of the SEB "double counted" the diffusion heat flux component. This conclusion was based on derivations starting with a general form of the energy equation. In addition, INSRP/RESP contends that the LMMS formulation omits a homogeneous reaction term. The final form of the SEB advocated by INSRP is the conventional approach, Equation [3-17].

Independent Review of the SEB: Dr. George Sutton, a pioneer in the development of carbon ablation models and the use of carbon composites for thermal protection, was the first choice of LMMS and INSRP/RESP to serve as a reviewer and provide an expert assessment of the SEB formulations.

Dr. Sutton documented his conclusions in an Interim and a Final Report to LMMS. In summary, his derivations led to the conclusion that in the LMMS SEB formulation diffusion is counted twice. He did not concur with Equation [3-16] or Equation [3-17]. Rather, he contends that the correct balance is obtained by omitting the diffusion heat flux component contained in the LMMS $\dot{q}$ term.

Computational Approach to Assess Effect of SEB: In order to quantify the effect of the SEB formulations on the predicted survival/failure of the GPHS aeroshell, the transient aerothermal response of the module was recomputed for the steep (γ = -90°) and shallow (γ = -7°) trajectories using the LMMS, INSRP, and Sutton forms of the SEB. The computations were performed at the stagnation point using a version of REKAP that has been modified to obtain the net heating and ablation rates from CFD generated tables. Use of the one-dimensional REKAP code reduces the computational time for a trajectory to a few seconds compared to several hours required by the three-dimensional SINRAP code. The various forms of the SEB are constructed using existing CFD results that contain all of the required terms.

Effect of SEB on the Steep Trajectory: Previously reported analyses show that the GPHS module in the FOS orientation will fail structurally at approximately 1.9 sec. The module temperature and recession predictions for this analyses were obtained using the SINRAP

code and based on the LMMS SEB formulation. Figure 3-9 shows the surface temperature history (from the REKAP code with CFD) that results from the use of the three proposed SEB formulations. The temperatures for the Sutton form of the SEB are low compared to the LMMS and INSRP solutions. The LMMS and INSRP temperatures are relatively close. The temperature at 2.0 sec from the previous 3-D SINRAP solution is also shown in Figure 3-9. Both the LMMS and INSRP solutions at 2.0 sec match the SINRAP prediction.

Recession histories are shown in Figure 3-10. The Sutton SEB leads to considerably less recession. The LMMS and INSRP results are similar and both slightly overpredict recession compared to the 3-D SINRAP solution.

Effect of SEB on the Shallow Trajectory: As previously reported, the GPHS module is predicted to survive the shallow trajectory. Figure 3-11 shows the predicted surface temperature histories using the three SEB forms in the 1-D REKAP code. The Sutton SEB again leads to very low temperatures. The REKAP run with the Sutton SEB was terminated

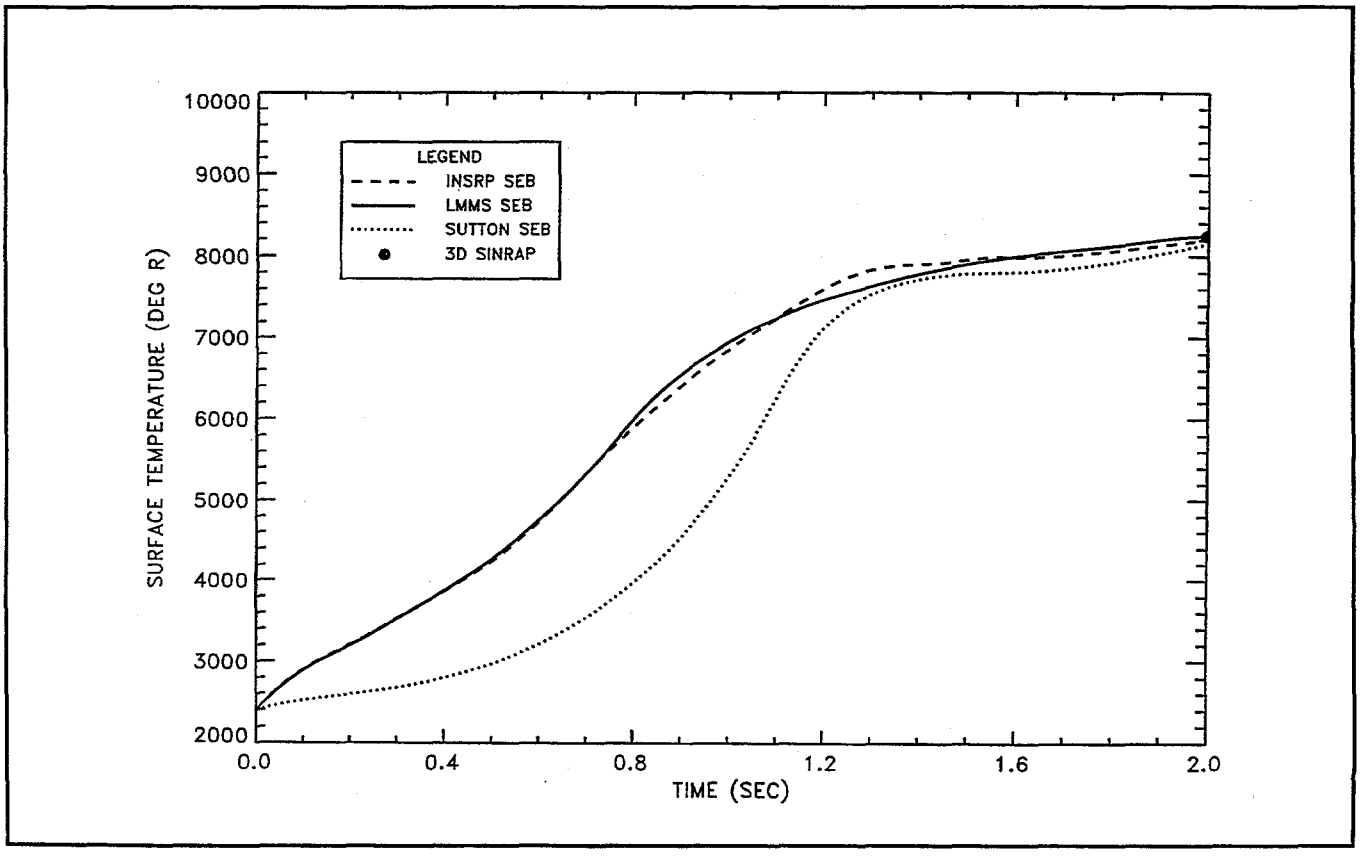

Figure 3-9. Effect of SEB Formulation on the GPHS Surface Temperature History along the Steep Trajectory

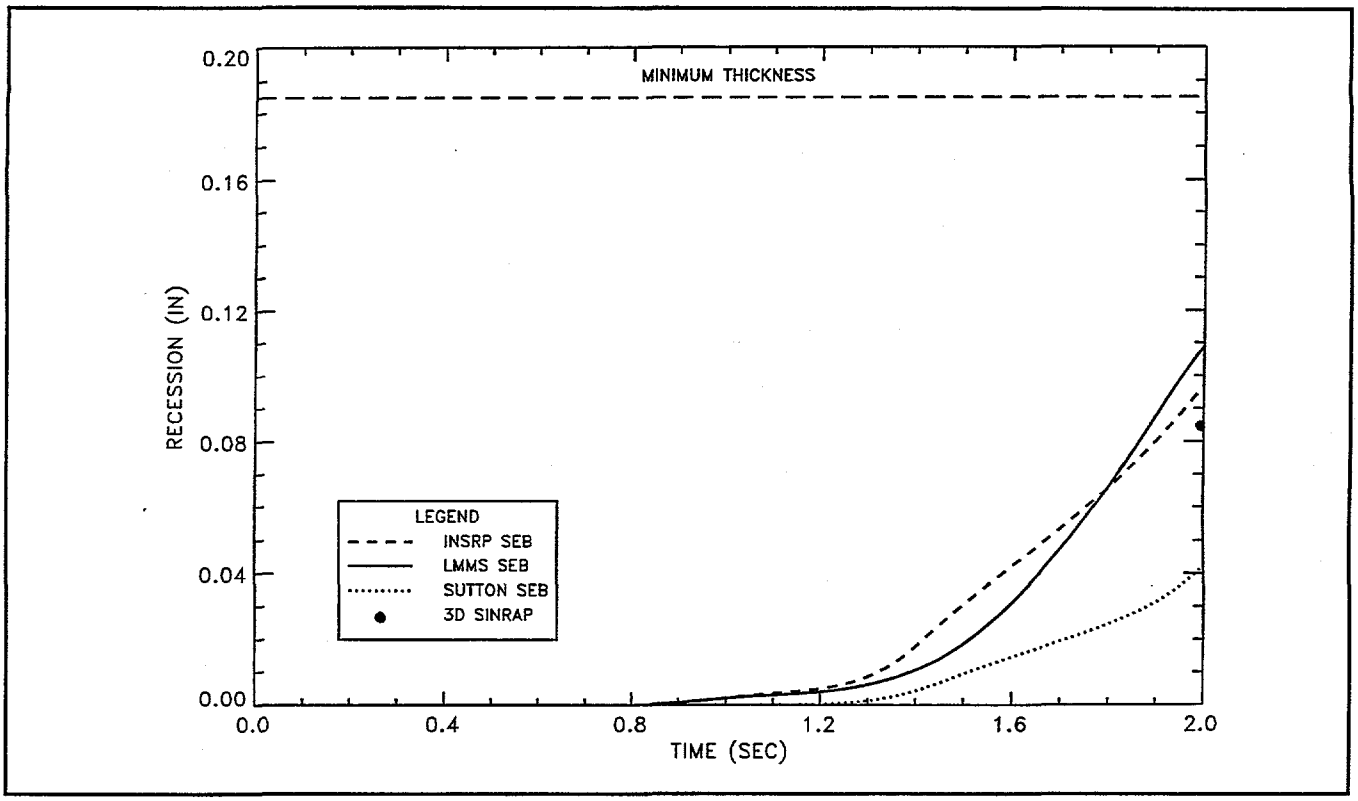

Figure 3-10. Effect of SEB Formulation on the GPHS Recession History along the Steep Trajectory (Not Adjusted for 3-D Effects)

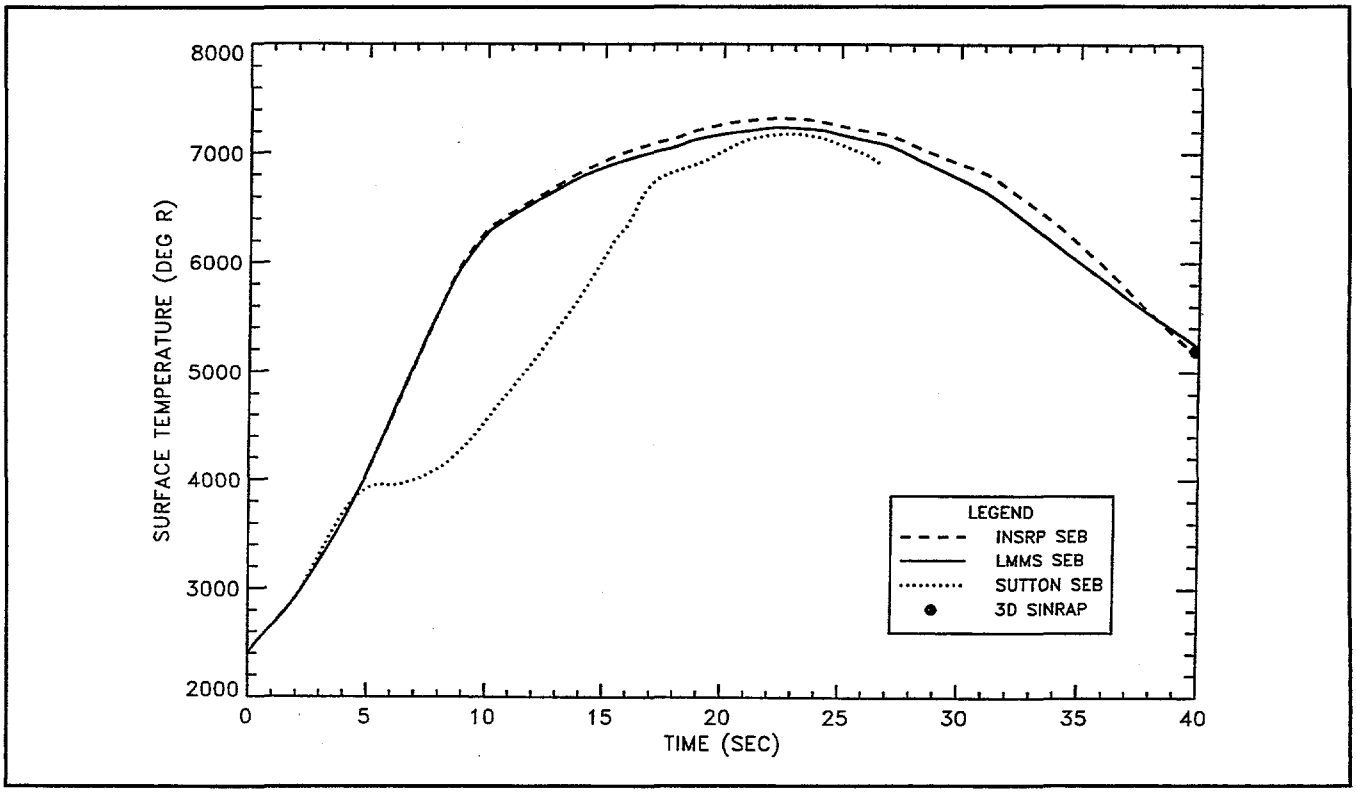

Figure 3-11. Effect of SEB Formulation on the GPHS Surface Temperature History along the Shallow Trajectory

at 27 sec because the low temperatures fell outside of the CFD database. The INSRP SEB causes slightly higher temperatures than the LMMS SEB over most of the trajectory. At 40 sec, both the LMMS and INSRP SEB solutions are very close to the temperature obtained using the 3-D SINRAP approach.

In Figure 3-12, the recession history from the 3-D SINRAP solution is compared to the 1-D REKAP prediction. As expected, the 1-D approximation leads to more recession (at most a 10% increase) than the full 3-D solution. To account for this effect, the REKAP recession results for the shallow trajectory, shown in Figure 3-13, have been adjusted downward following the trend shown in Figure 3-12.

As shown in Figure 3-13, use of the INSRP SEB causes more recession than the LMMS SEB. Differences in predicted recession increase along the trajectory. At 40 sec the INSRP SEB recession is about 32% greater than the recession obtained with the LMMS SEB.

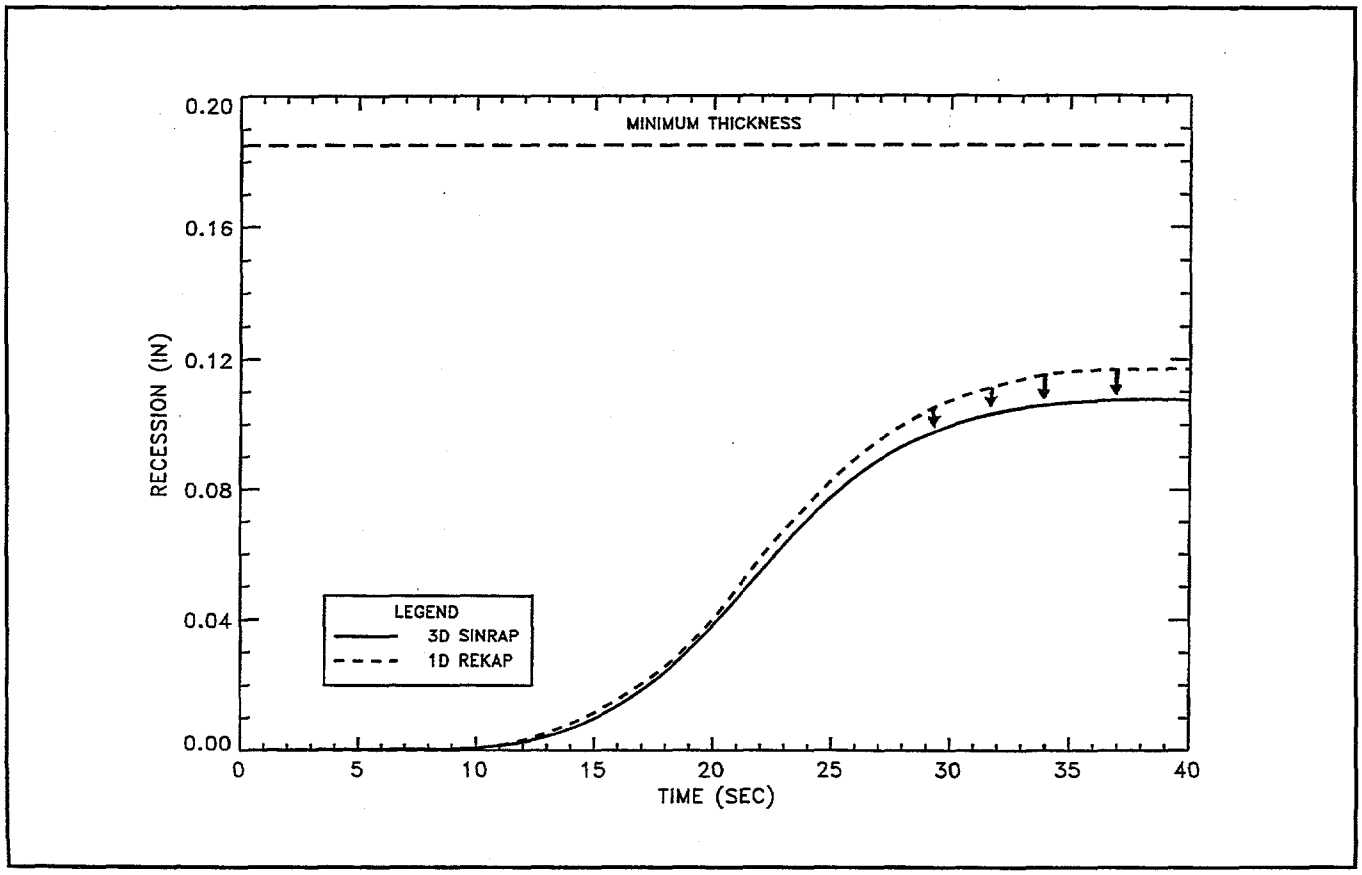

Figure 3-12. Comparison of 1-D REKAP with 3-D SINRAP Transient Heating Analysis along the Shallow Trajectory

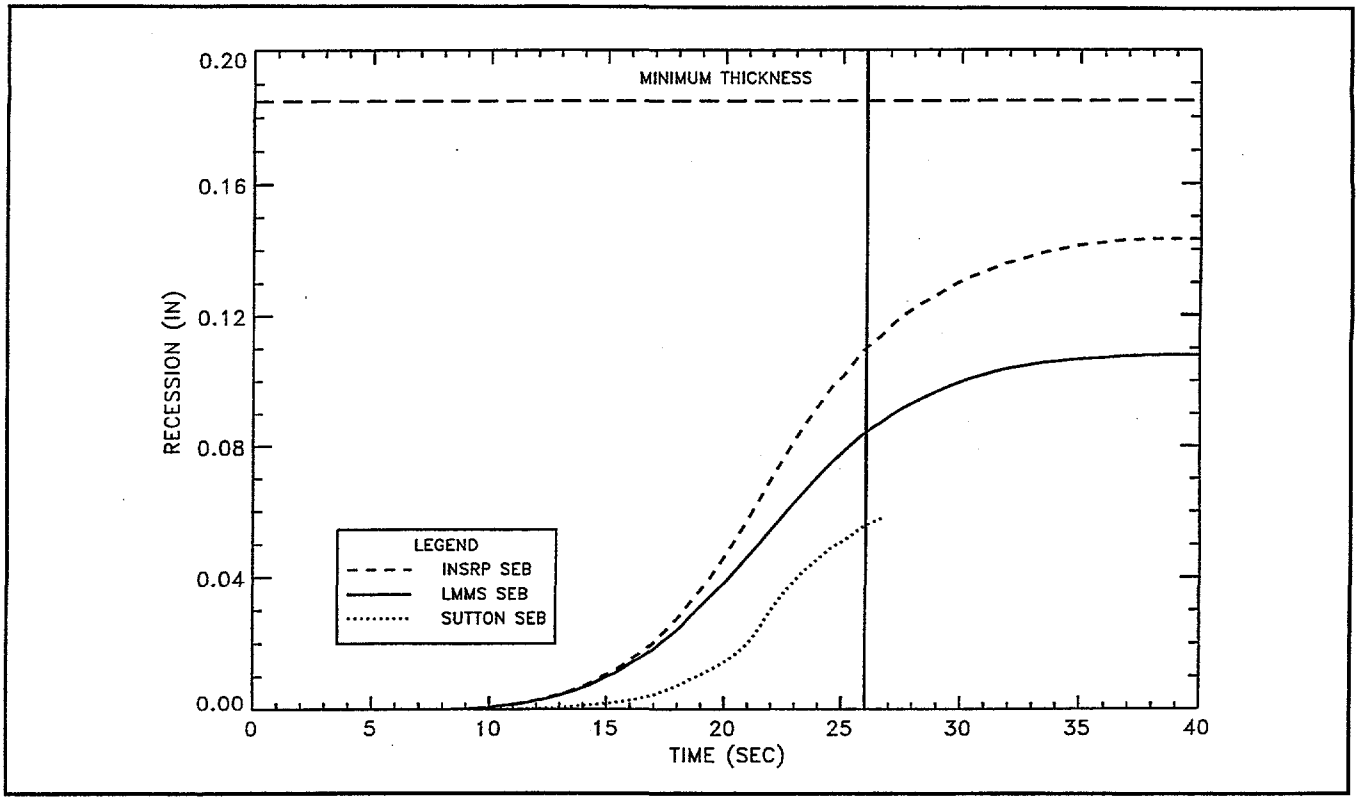

Figure 3-13. Effect of SEB Formulation on the GPHS Recession History along the Shallow Trajectory (Adjusted for 3-D Effects)

Conclusions: The REKAP code, modified to employ the CFD solution matrix, has proven to be a viable technique to rapidly estimate the thermal response of the GPHS module at the stagnation point. Use of the INSRP SEB (in lieu of the LMMS SEB) does not change previously reported conclusions for the steep and shallow trajectories. With either SEB, the module will fail structurally at approximately 1.9 sec on the steep trajectory. The module will survive the shallow trajectory, using the INSRP SEB even though the recession is greater than that predicted using the LMMS SEB. The module survives because the minimum factor of safety, which occurs at peak load, is reached at 26 sec (marked by a vertical line in Figure 3-13). As shown in Figure 3-14, beyond 26 sec the load rapidly decreases so that, despite thinning of the aeroshell, structural failure is not expected. However, the conservative estimate for the critical reentry path angle of $\gamma = -16^{\circ}$, based on use of the LMMS SEB, is less conservative with the INSRP SEB.

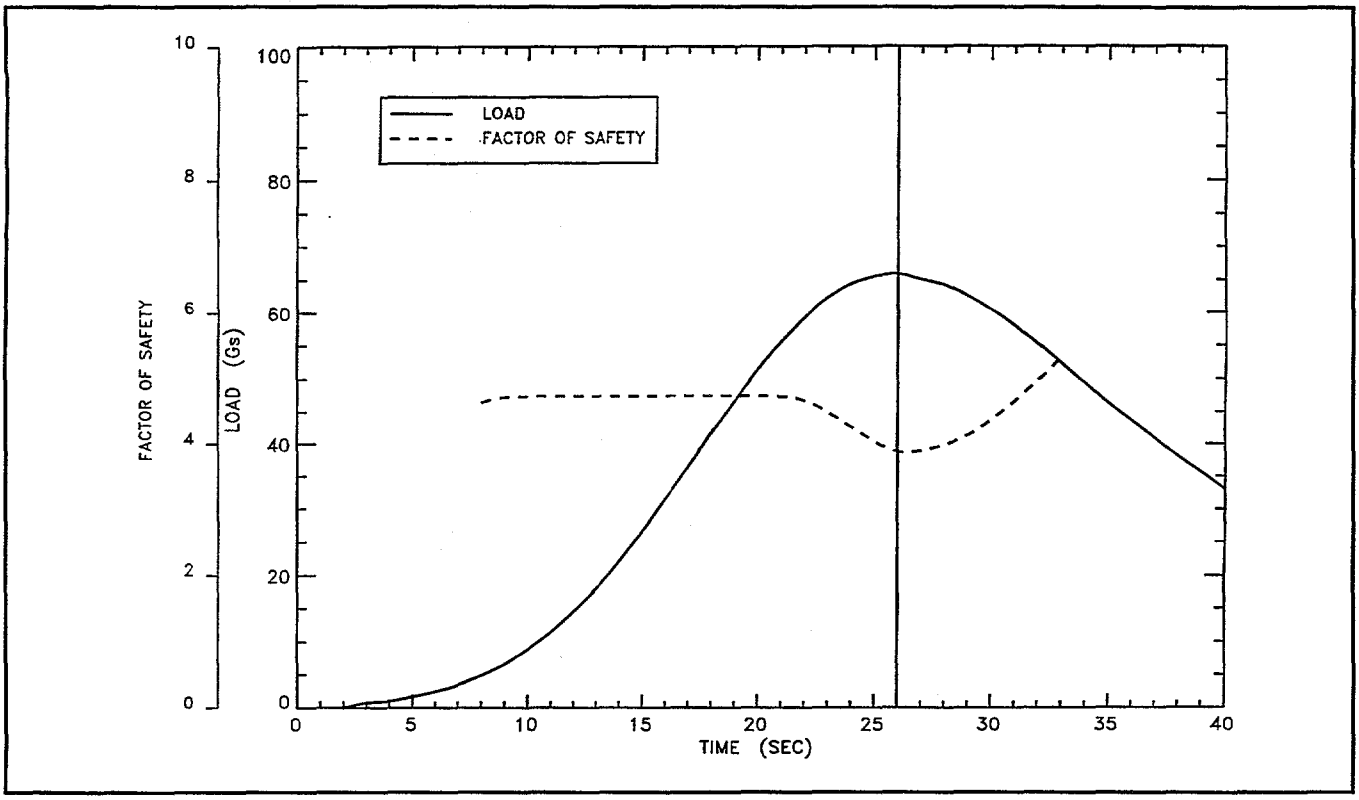

Figure 3-14. Factor of Safety (X-Direction Strain) and Load History along the Shallow Trajectory

Out-of-Orbit Analyses

PIR #144 for the Module Impact Model (MIM) was prepared and issued on 18 March 1997. This model uses subroutines from LASEP-T for calculating source terms for out-of-orbit reentry accident cases. The MIM code was delivered to INSRP Power Systems Subpanel.

Thermostructural Uncertainty Analysis

Approach: Mechanical material properties are the most significant uncertainty associated with the thermostructural reentry analysis. Test data for the FWPF material used for both the GPHS aeroshell and the GIS are limited to temperatures below 6000°F, while both components can achieve temperatures approaching 8000°F during various EGA reentry scenarios. As a result, it was necessary to extrapolate FWPF material properties to the upper limits of the temperature range based on data trends, a limited amount of data for graphite at 6200°F, and a basic understanding of carbon-carbon material behavior at elevated temperatures. This extrapolation introduces the largest amount of uncertainty into the thermostructural reentry analysis and, as a result, became the focus of uncertainty work in this area.

The difficulty in assessing the uncertainty in the FWPF material properties is that a number of these properties directly impact the capability of the aeroshell, such as material strength, primary and secondary moduli, yield strength, and thermal expansion coefficient. These properties are all correlated to some extent because they are based on the micromechanics of a densified woven fiber composite. In order to treat material uncertainty in a manageable form, a simplified approach to assessing material variations was used. Essentially, two additional material property databases were created for the FWPF material. These databases were of the same nonlinear form as the nominal material property database created for the baseline analyses, but represent a correlated set of "high" and "low" properties based on 2-sigma uncertainties. The methodology for deriving material properties for both of these datasets was presented in previous reports.

Since the nominal analysis of the aeroshell indicates definitive survival for the shallow trajectory and failure for the steep trajectory, the focus of the uncertainty work was the intermediate trajectory where aeroshell failure/survival is marginal. Specifically, the goal was to assess how much impact the material property uncertainties have upon the critical angle for aeroshell failure that was nominally established as -16 degrees for the FOS attitude and -21 degrees for the random tumbling reentry. A two-fold methodology was utilized to assess this impact. The analysis results (stresses and strains) for the intermediate trajectory utilizing the nominal material properties (moduli, yield strengths, and thermal expansion coefficients) were evaluated against the material allowable strengths from the high and low datasets. This directly established the variation of aeroshell factor of safety with material allowable strengths. Then, the critical intermediate analysis cases were analyzed utilizing the full high and low correlated material property datasets, including material allowables. This approach provided a more realistic assessment of how correlated material property variations could impact aeroshell factors of safety. The results from these two analysis approaches were utilized concurrently to provide an estimate of the uncertainty in the critical path angle threshold for aeroshell failure.

Results: The first set of uncertainty analysis results were based upon uncorrelated material allowables, where stress and strain predictions utilizing the nominal material databases were evaluated against material allowables from the 2-sigma high and low

databases. The intermediate trajectory analysis results were assessed utilizing this approach, with a prediction of aeroshell failure at t=5.0 secs and t=6.0 secs for the low and high allowable datasets. These failure times correspond to acceleration loads of 125 Gs and 202 Gs for the respective datasets. Correlating these maximum acceleration loads with reentry path angles as was done for the nominal analysis case results in a range of critical reentry threshold path angles from 12 to 16 degrees. These angles are based on the intermediate 20 degree reentry temperature profiles; however, the actual temperature profiles generally will be lower with less thermal gradient for lower path angles, resulting in increased structural capability. As a result, the critical path angle range was adjusted upwards 2 degrees at the low end and 1 degree at the high end. The resulting prediction of the critical path angle range using this uncertainty approach was 14 to 17 degrees.

The second thermostructural uncertainty analysis approach was to perform analysis for the intermediate trajectory using the fully correlated 2-sigma high and low material property databases. This approach is based on the assertion that the micromechanics that cause a woven fiber composite to have higher (or lower) than nominal stiffness will also result in higher (or lower) yield and ultimate strengths. The minimum factors of safety resulting from these analysis cases were plotted to determine failure loads. The minimum factors of safety for X direction stress and strain are plotted in Figures 3-15 and 3-16, respectively, with the nominal, high, and low dataset predictions included for comparison. Similar plots for Y direction strain and Z direction strain are included in Figures 3-17 and 3-18. Several additional analytical cases beyond what was utilized for the nominal analysis were required to better define failure loads for both the high and low material datasets. In addition, for the high material property dataset, an analysis run at t=6.2 seconds could not be completed due to aeroshell structural failure and subsequent numerical divergence. As can be seen from the analysis data in the factor of safety plots, the correlated 2-sigma low dataset indicates aeroshell failure at approximately t=4.85 seconds, while the prediction for the 2-sigma high dataset is t=6.1 seconds. These times correspond to loads of 115 Gs and 220 Gs and translate to a critical path angle range of 11 - 17 degrees. Applying the same temperature profile correction discussed above results in a prediction of the critical reentry path angle threshold of 13 to 18 degrees using this approach.

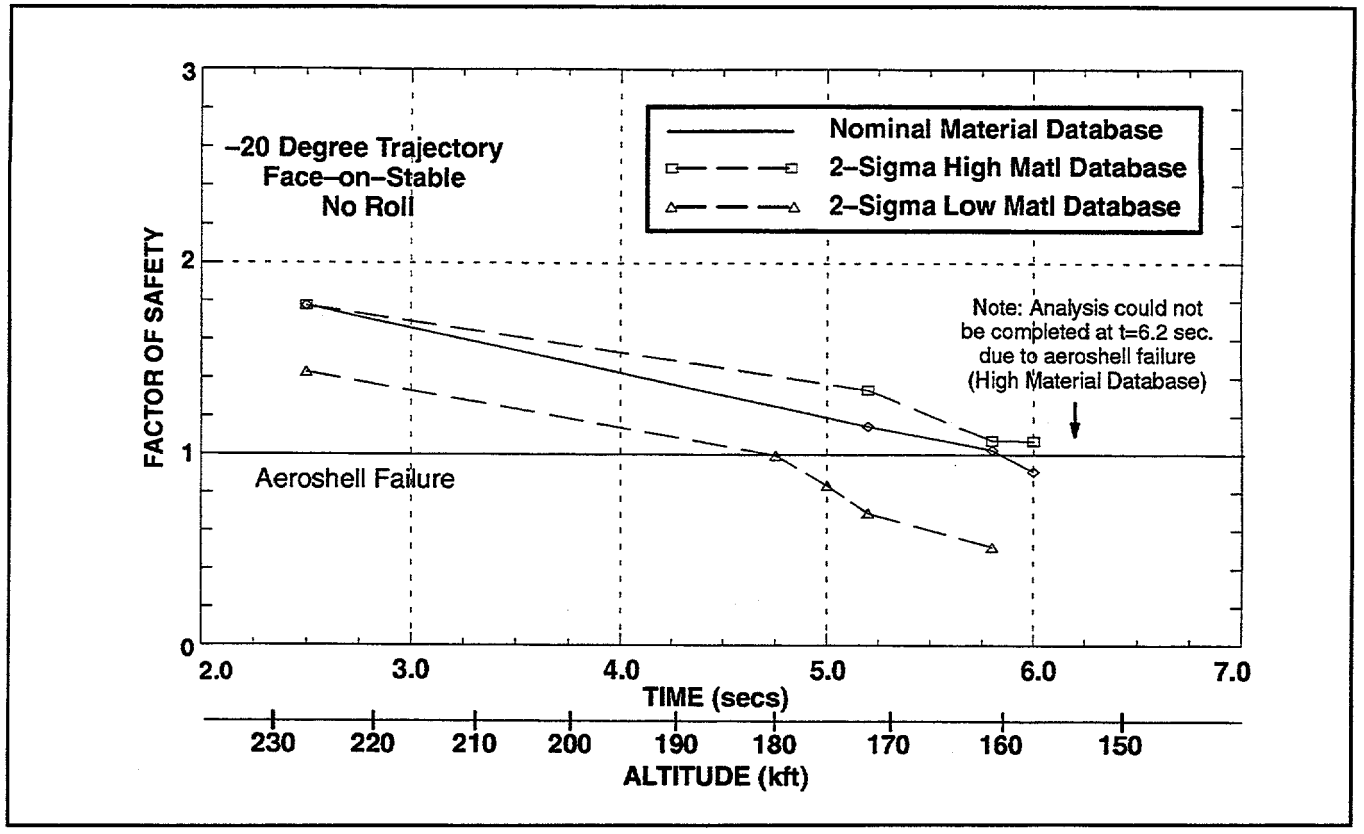

Figure 3-15. Minimum Factor of Safety vs. Time – X Direction Stress - Aeroshell

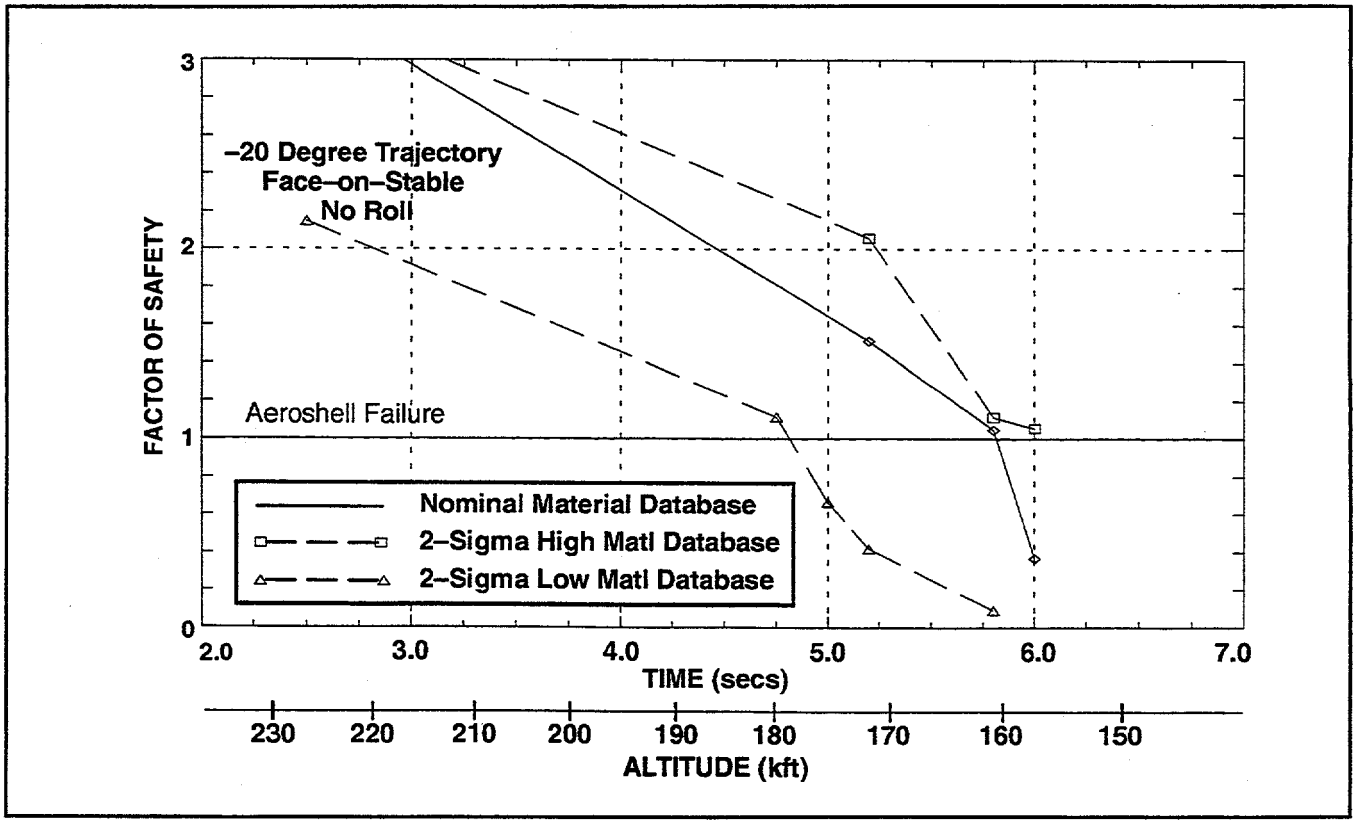

Figure 3-16. Minimum Factor of Safety vs. Time – X Direction Strain - Aeroshell

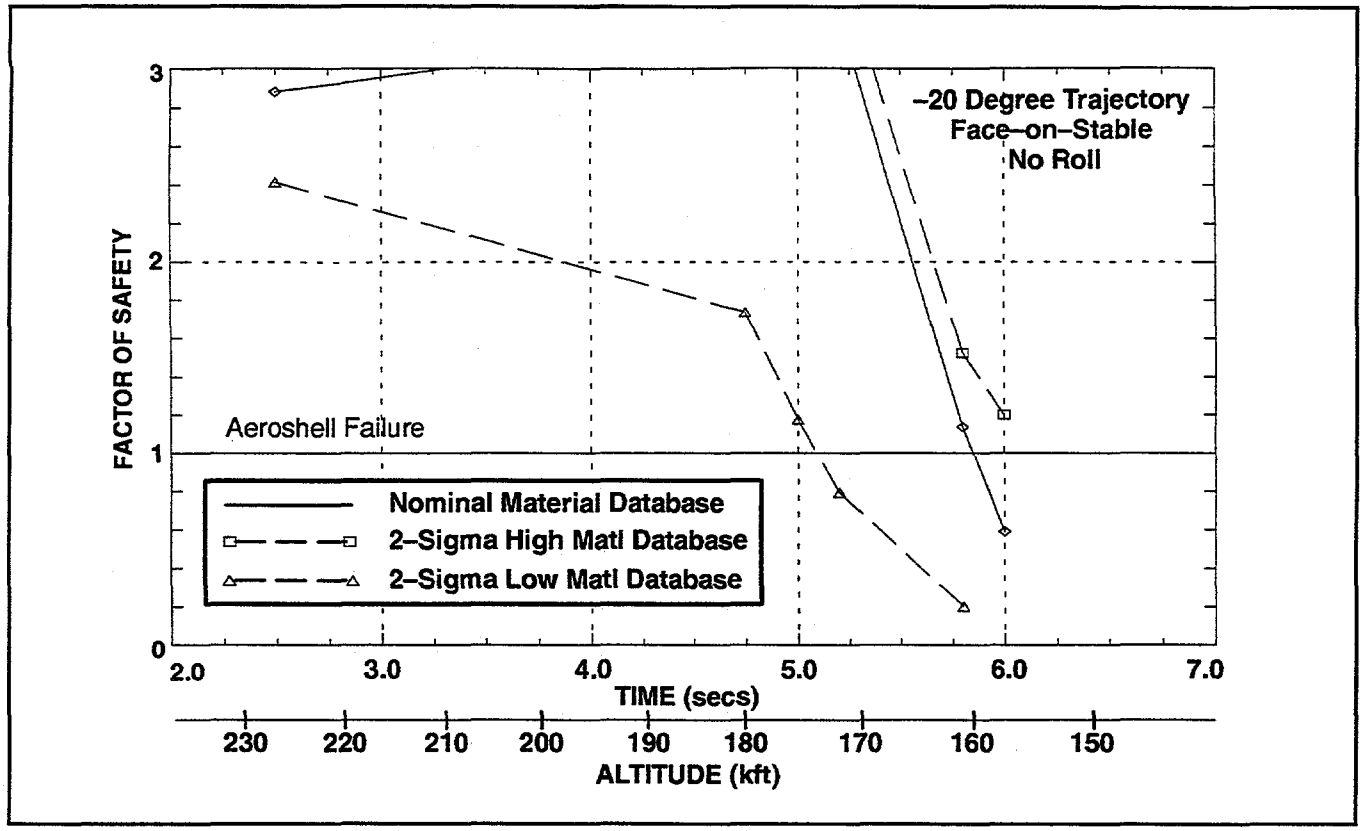

Figure 3-17. Minimum Factor of Safety vs. Time – Y Direction Strain - Aeroshell

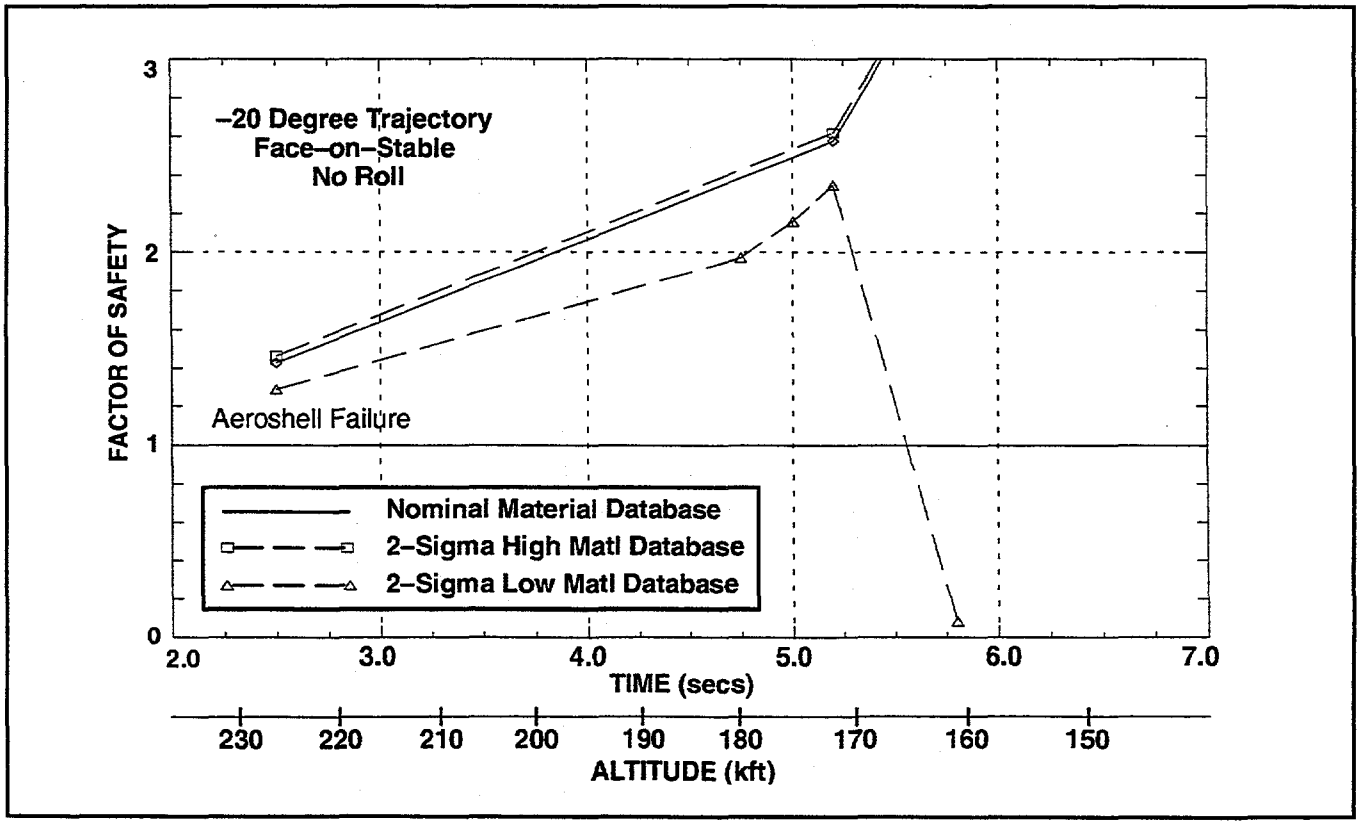

Figure 3-18. Minimum Factor of Safety vs. Time – Z Direction Strain - Aeroshell

The uncertainty analysis results for the two different approaches were fairly similar and were combined to produce a single prediction. The critical path angle threshold for the GPHS aeroshell is estimated to range from 13 to 18 degrees, based on thermostructural analysis uncertainty only. This range was combined with the uncertainty predicted for the aerothermal analyses to generate an overall uncertainty bound for the critical failure path angle threshold.

Consequence and Risk Analysis

Three principal areas of progress identified for this period are:

1) The completion of risk analyses for the FSAR, providing both variability and uncertainty results for the primary launch opportunity.
2) The variability-only analysis for the consequence of launch phase accident cases, in response to updates of accident environments as defined in Revision B of the Databook.
3) The Earth swingby consequence analysis for the secondary launch opportunity.

FSAR Analysis

The risk analysis as presented in the FSAR encompasses a substantial number of consequence analyses performed for accident cases considered in various phases of the Cassini mission.

For the variability-only analysis, each accident case in phase 0 (pre-launch) and phase 1 (launch) was evaluated with 30 LHS observations to obtain the distribution of consequence results. Each LHS observation involved a sampling of three release fuel clusters and ten weather-day clusters, resulting in 30 SPARRC analyses. This detailed analysis process was performed for accident cases 0.1, 1.1, and 1.3. The remaining accident cases which have low probability of release or small contributions to the total mission risk were evaluated with a scaling method.

For the out-of-orbit reentry accidents in phases 3-8, a combined total of 900 LHS/SPARRC analyses were performed. Compared to previous mission analyses, several refinements were implemented, including:

1) An updated mean exposed rock fraction was used to calculate the number of GPHS modules releasing fuel upon rock impact;

2) A multinomial distribution sampling was used to predict the combination of breached modules with the population density classes within the receptor cell. For the transport analysis at ground level, the EPA/DOE adopted average wind speeds corresponding to typical atmospheric dispersion conditions were used instead of the previously supplied HNUS database.

Two processing levels were considered for EGA inadvertent reentry accidents. In the first level, the end states of GPHS modules are predicted, the consequence analysis for air release source term is performed, and a consequence result is calculated for various ground impact conditions normalized for 1 affected person; 2) In the second level, the combination of breached GPHS modules at rock/soil impacts and population density classes is calculated, based on a multinomial distribution sampling. Once the potential consequences from various release types are obtained, the integration of results is performed. The 300 LHS observations performed for the EGA variability-only analysis have produced over 10,000 point estimates of consequence results.

The uncertainty analysis started with a review of the consequence parameter distributions and several test runs performed to reveal the sampled values and the response of consequence models. This review consisted of an investigation of the sampled parameters relative to Sandia National Laboratory staff expectations as to the shape of these sample distributions, the substantiation for each distribution, and the investigation of parameter distributions that appear to be dominant contributors to the consequence uncertainty. A more uniform sampling result between defined quantiles has led to a change from cumulative linear sampling to continuous logarithmic sampling for a number of important parameters, including deposition velocity multiplier, inhalation dose conversion factor, urban and rural resuspension factors, and vertical diffusion of high atmospheric layers.

For the uncertainty analysis, each pre/early launch accident case, with 36 parameters/variables considered, was analyzed with 50 LHS observations to provide a total of 1500 SPARRC consequence results. Out-of-orbit and EGA accident cases, with 29 and 60 parameters/variables respectively, were analyzed with 300 LHS observations each. While an out-of-orbit observation requires only a single ground release analysis with SATRAP, an EGA observation potentially includes several types of release including air release at high altitudes and three other types of release at ground impact. Thus, an EGA

case requires all three SPARRC codes (SATRAP, GEOTRAP, and HIAD) for the consequence calculation. All uncertainty analysis results were presented in the form of CCDFs with 5%, 50% and 90% confidence levels. The importance of parameters in each accident case was quantified based on the ranking from a parallel regression analysis.

To assure the adequacy of the number of observations adopted for the uncertainty analysis, the consequence of several accident cases were re-evaluated with additional samplings. A comparison of results in terms of quantile values and CCDF curves revealed that only small differences exist between various analyses.

FSAR Addendum Analysis

Revision B of the Databook introduced significant differences in the definition of accident environments. Mainly, the new elements to be considered for launch phase accidents are the effects of the revised Centaur overpressure, the presence of SRMU fire plume, and SRMU coincident impact source terms. These changes, in terms of characteristics of released source terms and transport analysis, have been successfully implemented in the consequence analysis process and a new set of consequence results were provided for the FSAR Addendum.

The key modeling detail for the updates, not present during the FSAR, was the diffusion of source terms in the presence of a large areal burning zone of solid fuel fragments. This particular effect is required to be understood and modeled appropriately because virtually all accident cases in the launch phase are associated with SRMU fire plume. Data from the Titan 34D accident (April 1986) and the recent Delta 2 accident (January 1997), such as video footage and meteorological conditions, were obtained to derive typical inputs for SRMU plume rise simulation. A calibration factor for the appropriate energy level input to PUFF (from Sandia National Laboratories) was derived based on plume rise heights calculated for both accidents. The semi-empirical Briggs' model was also reviewed and provided reasonable results. However, the PUFF code reflects better local meteorology conditions defined for each weather-day and was implemented for automation in the analysis process. Regarding the diameter of the burning zone, results from SRMU footprint simulations were examined along with video footage and pictures taken from the Delta 2 accident to determine an effective diameter defined as the "dense burning zone."

This zone is where individual plumes join together with a strong buoyancy, forming a well-mixed column for any potential source term released inside its volume. A nominal factor of 0.5 times the SRMU fragment footprint overall diameter was adopted for the dense burning zone diameter.

Due to the low conditional probability of SRMU coincident impacts in cases 1.1, 1.3, and 1.10, the source term was separated for SRMU and non-SRMU-induced groups, and two passes of consequence analyses were implemented. Thus, for each of these cases, a total of 60 LHS observations or 1800 SPARRC analyses were performed. Accident cases 0.0 and 1.13 were analyzed with a single pass of analysis (30 LHS observations) because their source terms were evaluated with a single LASEP-T simulation. Note that case 0.0 applies to phase 0 (pre-launch) and represents a composite case combining the environment threats defined for the former cases 0.1 (On-Pad Explosion) and 0.2 (On-Pad Explosion with SRMU Aft Segment Impact). A number of other cases (1.2, 1.4, 1.6, 1.8, and 1.9) with low probability of release were analyzed without the SRMU-induced source term.

In preparation for the FSAR Addendum analysis, several modifications were implemented for the SPARRC codes in order to provide a higher level of detail of the consequence result outputs. The new features include:

- Ground contamination at 4 different levels, 0.2, 0.6, 1.2, and 2.4 $\mu Ci/m^2$ are provided in parallel with the current tabular output form, 5 bins per decade, for land, water, marsh and ocean. For accidents in the KSC/CCAS vicinity, contamination of agriculture lands such as citrus land and crop land are also evaluated.
- The maximum individual dose, affecting at least one person, is separated from the outputs of potential individual doses for easier reference and evaluation.
- The dose due to inhalation during cloud passage is adjusted for the on-site workers located indoors. Previously, this dose was over-estimated because a total of three shifts was used.
- For health effects evaluation, the fraction of collective dose from exposure above 0.2 Gy (400 rem) is reported if applicable.

In an effort to determine possible criteria for launch constraints and to validate the adopted weather categorization, case 1.1 without SRMU source term was re-analyzed. In order to obtain a complete sampling of the eight weather categories, 60 LHS observations or 1440 SPARRC analyses were performed. Although the exact favorable meteorological

conditions were not compiled, these results prove that the current categorization scheme is a good approach to assign relative importance of weather-day groups and an adequate sampling was performed.

VEEGA Analysis

A PIR was issued to document the consequence and risk results evaluated for inadvertent reentry during the Earth swingby phase of the Venus-Earth-Earth gravity assist trajectory (VEEGA) in the secondary launch opportunity. Two Earth swingbys are planned and therefore two separate analyses were performed. The source terms from all release types are assumed to be identical with the primary opportunity swingby (VVEJGA) although a lower swingby velocity is predicted (17.0 km/s for VEEGA as compared with 19.3 km/s for VEEJGA).

For this activity, a post-processor code was generated to determine the contribution from various release types in the VEEGA/VVEJGA consequence analysis. This code also provides a detailed description of the results such as mean health effects of each release type, contribution of consequence from ground impacts in different population density classes, and the number of sampled trials for each release type.

Task 4

Qualified Unicouple Fabrication

TASK 4 QUALIFIED UNICOUPLE FABRICATION

The remaining efforts in Task 4 are associated with testing of 18 couple modules. Test temperatures and life test hours are shown in Table 4-1.

Table 4-1. Test Temperatures and Life Test Hours

Module	Unicouple Source	Test Temperature Hot Shoe	Status as of 30 March 1997
18-10	Early Qualification Lot	1135°C	10,400 Hours Performance Normal Test Terminated October 1994
18-11	Full Qualification Lot	1135°C	26,769 Hours Performance Normal
18-12	Early Flight Production Lot	1035°C	22,858 Hours Performance Normal

18 Couple Module Testing

Two modules remain on life test. Testing of module 18-10 was terminated at the end of October 1994 after 10,400 hours.

Module 18-11 has accumulated an additional 4,097 life test hours during this reporting period and has reached 26,769 hours (3.05 years) of accelerated life testing. Its performance continues to provide added confidence that normal unicouple performance can be expected from the flight RTGs during the Cassini mission.

Module 18-12 has accumulated an additional 4,368 life test hours and has reached 22,858 hours (2.61) years at design temperature levels and continues to show normal performance.

Module 18-11 was shut down under controlled conditions for regeneration of the cryopump in November. Testing of module 18-12 continued without interruption during this reporting period.

Module 18-11 (1135°C)

On 30 March 1997, the module reached 26,769 hours at the accelerated hot shoe temperature of 1135°C. Measured performance during this period continues to fall within the data base established by MHW and GPHS 18 couple modules.

The thermoelectric performance evaluation primarily studies the trends of the internal resistance and power factor. Figures 4-1 and 4-2 show these trends in comparison to module 18-8, the last module built during the GPHS program. Agreement is excellent and continues to provide a high degree of confidence that the GPHS unicouple manufacturing processes have been successfully replicated. The scatter in the data at the end of February (26,000 hours) was due to a faulty load transistor which has been replaced. Table 4-2 summarizes the initial and 26,769-hour performance data.

The isolation resistance trend between the thermoelectric circuit and the foil is shown in Figure 4-3 along with modules from the MHW and GPHS programs. The isolation resistance plateaued at about 1000 ohms between 6,000 and 7,000 hours. It then started a slow decrease and is presently at 351 ohms. A similar plateau and gradual decline were observed in MHW module SN-1. At the accelerated temperature of 1135°C the same amount of sublimation occurs in about 1,650 hours of testing as would occur in a 16-year Cassini mission.

Consequently, approximately 16.2 times as much sublimation has occurred during the test duration of module 18-11 as will occur during the Cassini mission. The module performance, therefore, confirms the adequacy of the silicon nitride coating on the qualification unicouples.

Individual Unicouple Performance: The performance of individual unicouples and rows of unicouples continues to be observed. Table 4-3 shows the room temperature resistance changes and the internal resistance changes observed during operation for each of the six rows and for individual unicouples in Rows 2 and 5. The unicouples continue to perform within a narrow band.

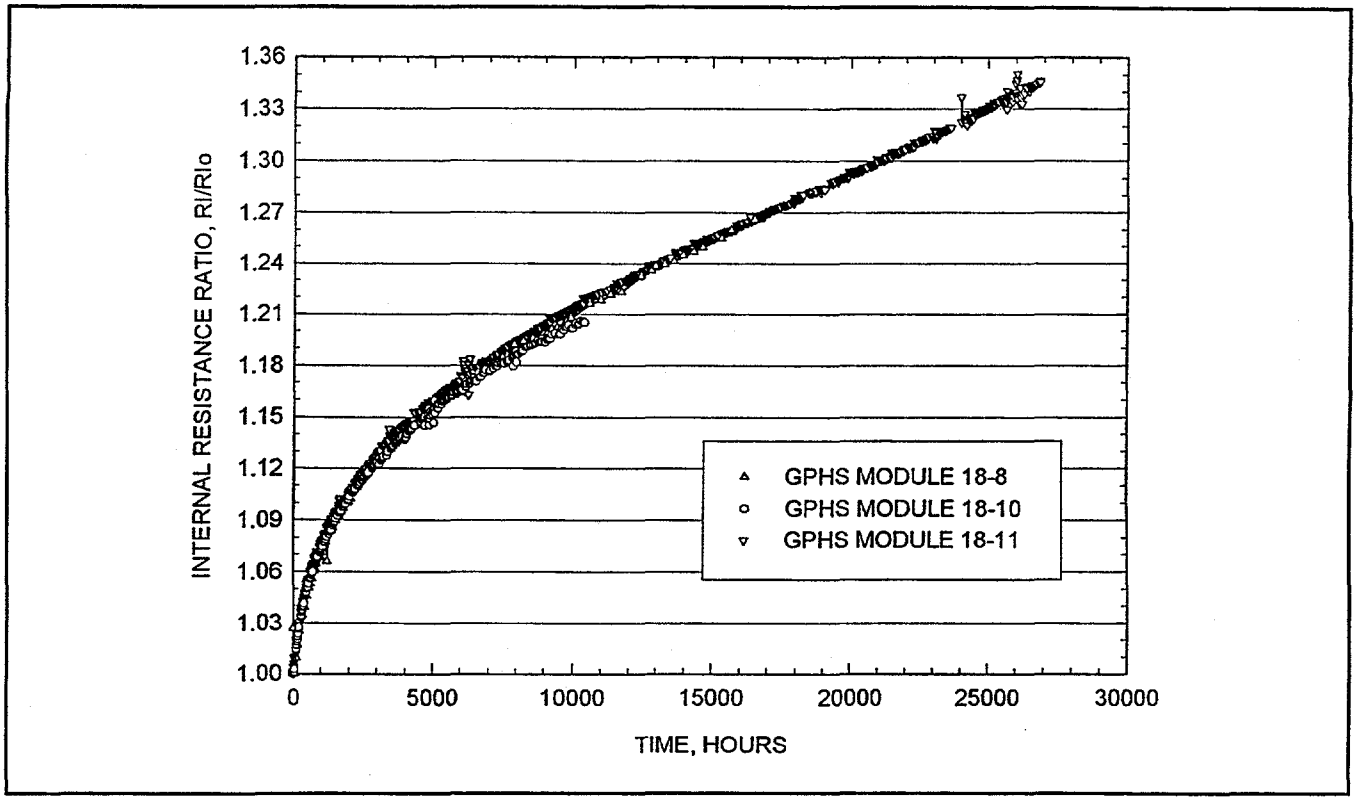

Figure 4-1. Internal Resistance Ratio Versus Time (Modules 18-10, 18-11, GPHS Module 18-8) – 1135°C Operation

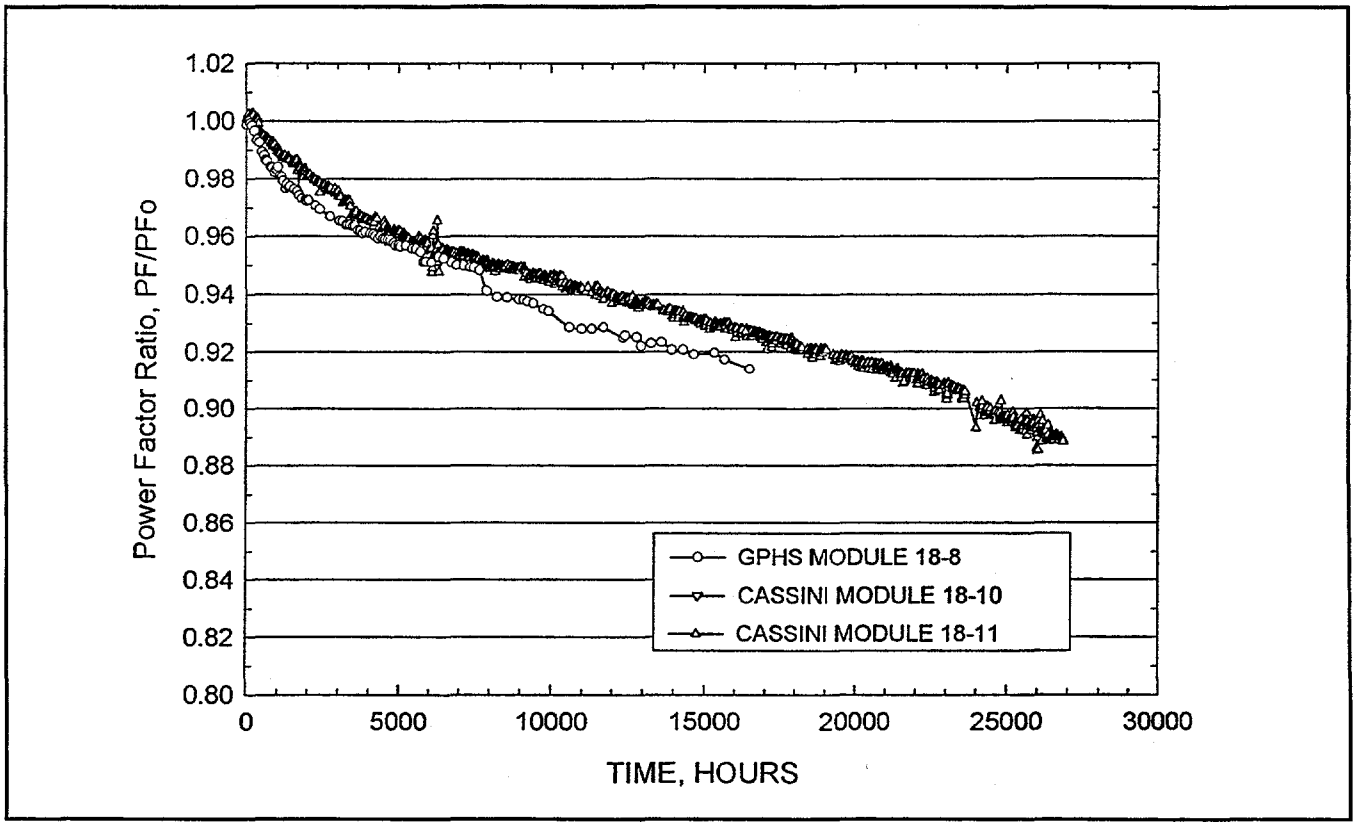

Figure 4-2. Power Factor Ratio Versus Time (Modules 18-10, 18-11, GPHS Module 18-8) – 1135°C Operation

Table 4-2. Comparison of Initial and 26,769 Hour Performance of Module 18-11 at 1135°C

	Initial 2/2/94	t = 52 Hours V_L = 3.5V 2/4/94	t = 26,769 Hours 3/30/97
Heat Input, Watts	190	192.9	193.6
Hot Shoe, °C Average	1137.8	1137.5	1105.0
Hot Shoe Range, °C	5.4	5.2	11.0
Cold Strap, °C Average (8 T/Cs)	311.9	314.3	303.1
Cold Strap Range (8T/Cs)	2.6	2.5	2.5
Cold Strap Average (12 T/Cs)	306.5	308.9	298.0
Cold Strap Range (12 T/Cs)	20.1	20.3	18.8
Load Voltage, Volts	3.895	3.499	3.479
Link Voltage, Volts	0.108	0.121	0.093
Current, Amps	2.842	3.174	2.682
Open Circuit Voltage, Volts	7.140	7.160	7.576
Normalized Open Circuits (8T/Cs)	6.319	6.359	6.933
Normalized Open Circuits (12 T/Cs)	6.276	6.316	6.887
Average Couple Seebeck Coefficient (12)	498×10^{-6}	501×10^{-6}	545.1×10^{-6}
Internal Resistance, Ohms	1.104	1.115	1.486
Internal Resistance Per Couple (Avg.)	0.0613	0.0620	0.0825
Power Measured, Watts (Load + Link)	11.375	11.492	9.63
Power Normalized, Watts (8 T/Cs)	8.909	9.065	8.02
Power Normalized, Watts (12 T/Cs)	8.789	8.942	7.92
Power Factor	40.452×10^{-5}	40.557×10^{-5}	36.00×10^{-5}
Isolation			
Circuit to Foil, Volts	-1.68	-1.36	-1.70
Circuit to Foil, Ohms	6.29K	5.95K	0.351K

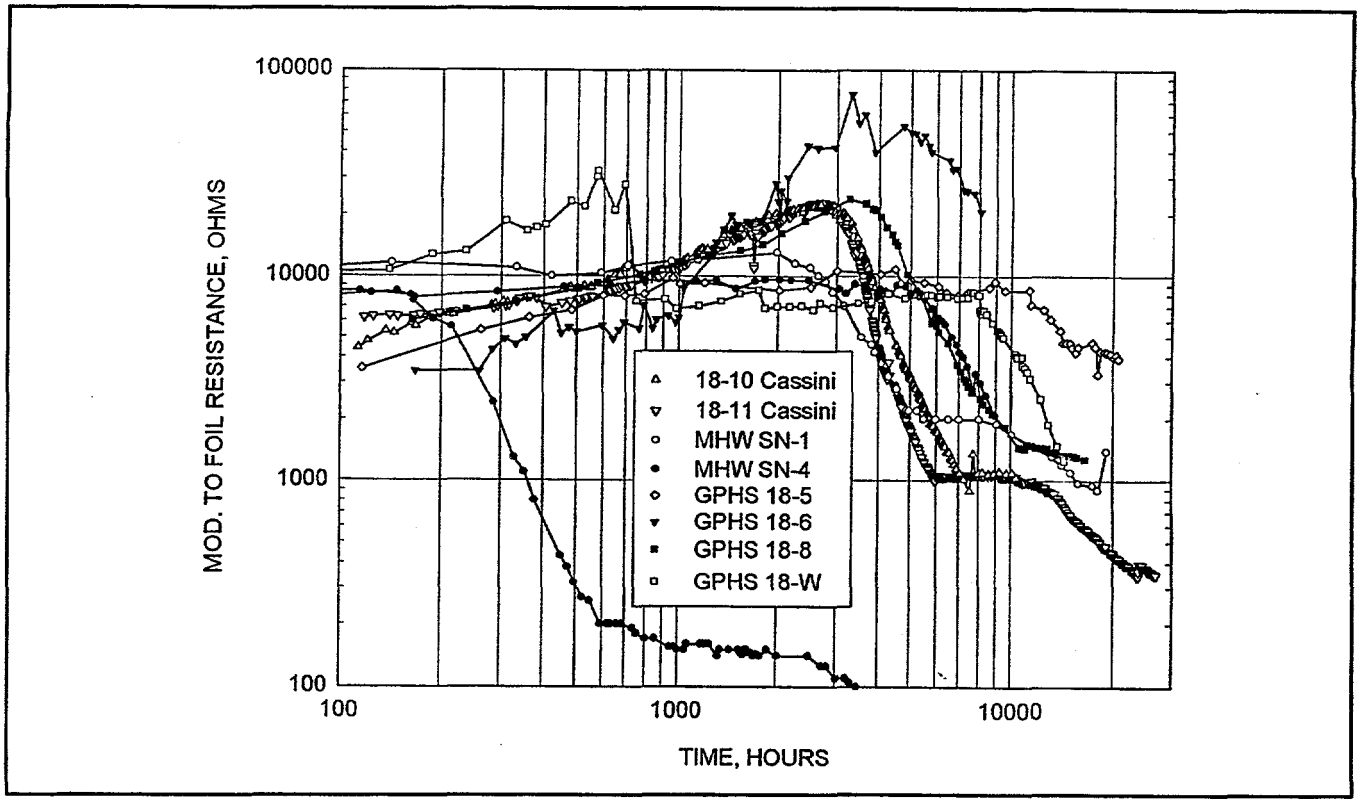

Figure 4-3. Isolation Resistance – Module Circuit to Foil (Modules 18-10, 18-11, GPHS Module 18-8) – 1135°C Operation

Table 4-3. Module 18-11 Internal Resistance Changes

Position	Serial #	2nd Bond Milliohm	Preassy Milliohm	Delta ri Milliohm	T = 0 Milliohm	T=1,509 Hours	Delta ri Milliohm	Percent Increase	T=26,769 Hours	Delta ri Milliohm	Percent Increase
1.0	H2006	22.50	22.10	-0.40							
2.0	H0507	22.40	21.90	-0.50							
3.0	H0512	22.7	22.20	-0.50							
					182.30	199.70	17.40	9.54	245.80	63.50	34.83
4.0	H0439	23.20	22.70	-0.50	62.30	67.90	5.60	8.99	83.60	21.30	34.19
5.0	H0587	22.50	22.40	-0.10	61.00	66.50	5.50	9.02	80.70	19.70	32.30
6.0	H0657	22.70	22.50	-0.20	61.40	67.30	5.90	9.61	82.10	20.70	33.71
					184.10	201.10	17.00	9.23	245.60	61.50	33.41
7.0	H0585	22.90	22.50	-0.40							
8.0	H0459	22.50	22.10	-0.40							
9.0	H0562	22.70	22.30	-0.40							
					185.70	203.20	17.50	9.42	254.10	68.40	36.83
10.0	H0248	22.70	22.30	-0.40							
11.0	H0163	22.90	22.40	-0.50							
12.0	H0282	22.70	22.40	-0.30							
					184.90	201.70	16.80	9.09	246.30	61.40	33.21
13.0	H0428	23.10	22.70	-0.40	62.10	67.90	5.80	9.34	82.90	20.80	33.49
14.0	H0326	22.60	22.00	-0.60	62.20	68.30	6.10	9.81	84.60	22.40	36.01
15.0	H0232	22.60	22.00	-0.60	60.90	66.60	5.70	9.36	84.70	23.80	39.08
					184.70	202.30	17.60	9.53	251.60	66.90	36.22
16.0	H0590	22.60	22.40	-0.20							
17.0	H0393	22.60	22.10	-0.50							
18.0	H0496	22.50	22.30	-0.20							
					184.20	201.40	17.20	9.34	245.20	61.00	33.12

Module 18-12 (1035°C Operation)

The module reached 22,858 hours at the normal operating temperature of 1035°C on 30 March 1997. Thermoelectric performance, as measured by internal resistance and power factor trends, continues to be normal as shown as Figures 4-4 and 4-5, respectively. Table 4-4 shows initial performance and the performance on 30 March 1997.

Isolation Resistance

The isolation resistance between the circuit and foil continues to show the normal trend as shown in Figure 4-6.

Individual Unicouple Performance

A review of the unicouple internal resistances and open circuit voltages indicates that all unicouples are exhibiting very similar behavior with time (See Table 4-5). The data for the six individually instrumented unicouples in Rows 2 and 5 are shown in Figure 4-7.

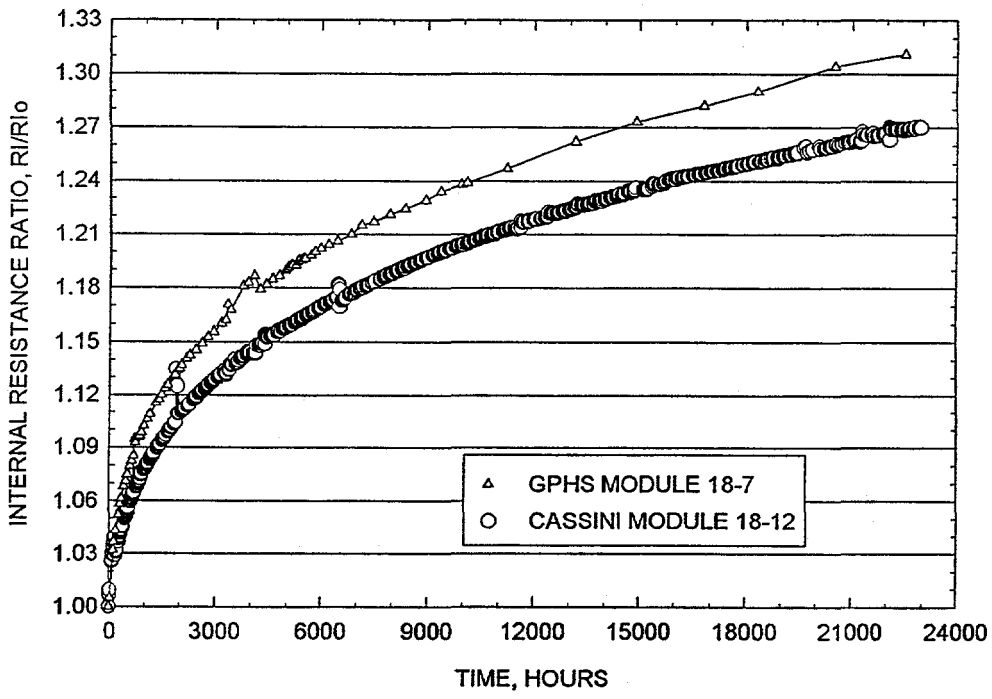

Figure 4-4. Internal Resistance Ratio Versus Time (Modules 18-12, and 18-7) – 1035°C Operation

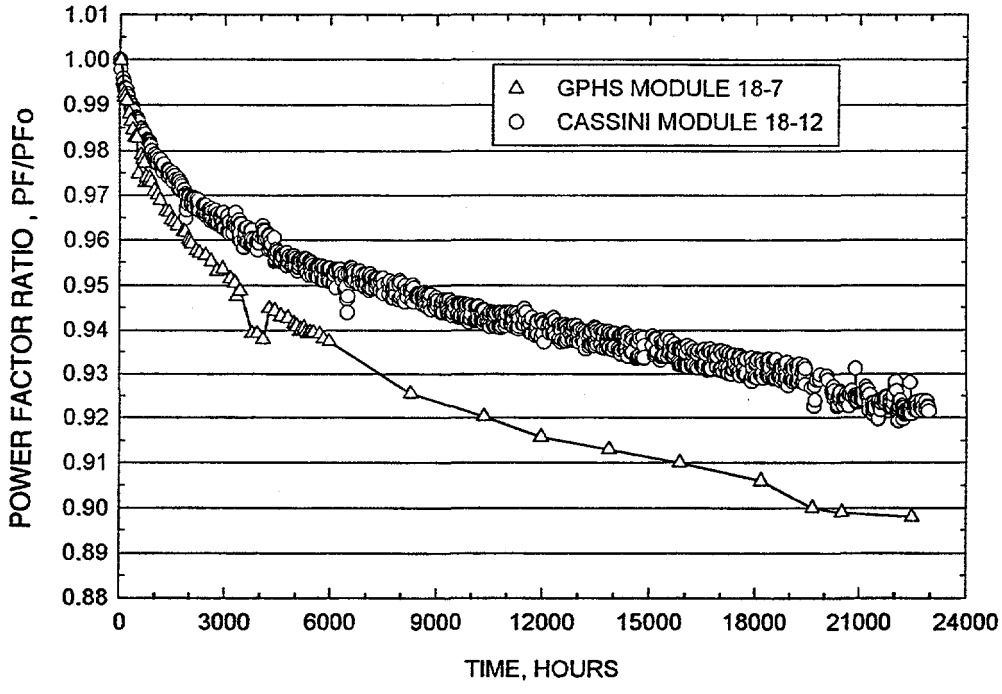

Figure 4-5. Power Factor Ratio Versus Time at Temperature (18-7 and 18-12) – 1035°C Operation

Table 4-4. Comparison of Initial and 22,858 Hour Performance of Module 18-12 at 1035°C

	Initial 6/16/94	t = 22,858 Hours 3/30/97
Heat Input, Watts	169.15	169.4
Hot Shoe, °C Average	1035.9	1025
Hot Shoe Range, °C	5.7	3.9
Cold Strap, °C Average (8 T/Cs)	287.1	280.1
Cold Strap Range (8T/Cs)	5.0	4.8
Cold Strap Average (12 T/Cs)	282.7	278.6
Cold Strap Range (12 T/Cs)	19.8	19.3
Load Voltage, Volts	3.578	3.498
Link Voltage, Volts	0.155	0.153
Current, Amps	2.548	2.436
Open Circuit Voltage, Volts	6.431	6.927
Normalized Open Circuit (8T/Cs)	6.307	6.830
Normalized Open Circuit (12 T/Cs)	6.268	6.816
Average Couple Seebeck Coefficient (12)	497×10^{-6}	538.2×10^{-6}
Internal Resistance, Ohms	1.053	1.345
Internal Resistance Per Couple (Avg.)	0.0588	0.0747
Power Measured, Watts (Load + Link)	9.510	8.89
Power Normalized, Watts (8 T/Cs)	9.146	8.63
Power Normalized, Watts (12 T/Cs)	9.011	8.50
Power Factor	42.06×10^{-5}	38.76×10^{-5}
Isolation		
Circuit to Foil, Volts	-1.71	-0.87
Circuit to Foil, Ohms	21.3K	175K

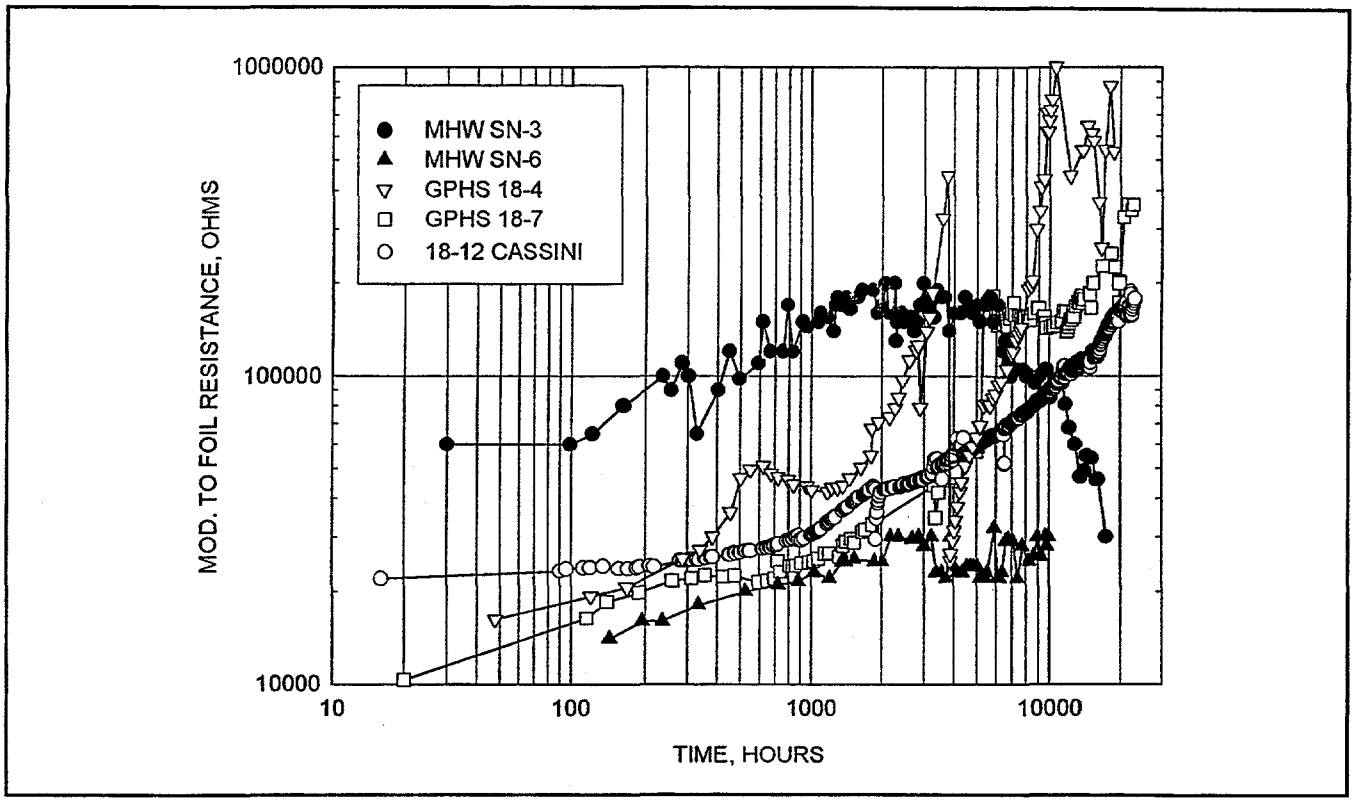

Figure 4-6. Isolation Resistance - Module Circuit to Foil (18-12, GPHS and MHW Modules) - (1035°C Operation)

Table 4-5. Module 18-12 Internal Resistance Changes

Position	Serial #	2nd Bond Milliohm	Preassy Milliohm	Delta ri Milliohm	T = 0 Milliohm	T=1,505 Hours	Delta ri Milliohm	Percent Increase	T=22,858 Hours	Delta ri Milliohm	Percent Increase
1.0	H2594	23.80	22.90	-0.90							
2.0	H2634	22.70	22.60	-0.10							
3.0	H2606	23.50	22.40	-1.10							
					176.80	192.10	15.30	8.65	222.20	45.40	25.68
4.0	H2168	22.20	21.70	-0.50	57.50	63.30	5.80	10.09	74.00	16.50	28.70
5.0	H2151	22.40	21.90	-0.50	57.40	62.90	5.50	9.58	73.10	15.70	27.35
6.0	H2256	22.20	21.70	-0.50	57.00	63.10	6.10	10.70	74.00	17.00	29.82
					171.20	188.60	17.40	10.16	220.40	49.20	28.74
7.0	H2597	24.40	23.20	-1.20							
8.0	H2680	22.60	23.00	0.40							
9.0	H2658	22.70	23.00	0.30							
					178.00	193.60	15.60	8.76	223.70	45.70	25.67
10.0	H1506	23.50	23.20	-0.30							
11.0	H1392	23.80	23.00	-0.80							
12.0	H1606	23.60	22.60	-1.00							
					176.20	193.40	17.20	9.76	224.60	48.40	27.47
13.0	H1344	23.60	23.50	-0.10	59.20	64.80	5.60	9.46	75.10	15.90	26.86
14.0	H1618	23.30	24.00	0.70	58.60	64.50	5.90	10.07	75.20	16.60	28.33
15.0	H1262	23.70	23.30	-0.40	59.40	65.00	5.60	9.43	75.40	16.00	26.94
					176.60	193.70	17.10	9.68	225.00	48.40	27.41
16.0	H1580	23.00	23.70	0.70							
17.0	H2127	22.80	22.10	-0.70							
18.0	H2113	22.90	22.20	-0.70							
					174.50	191.30	16.80	9.63	222.50	48.00	27.51

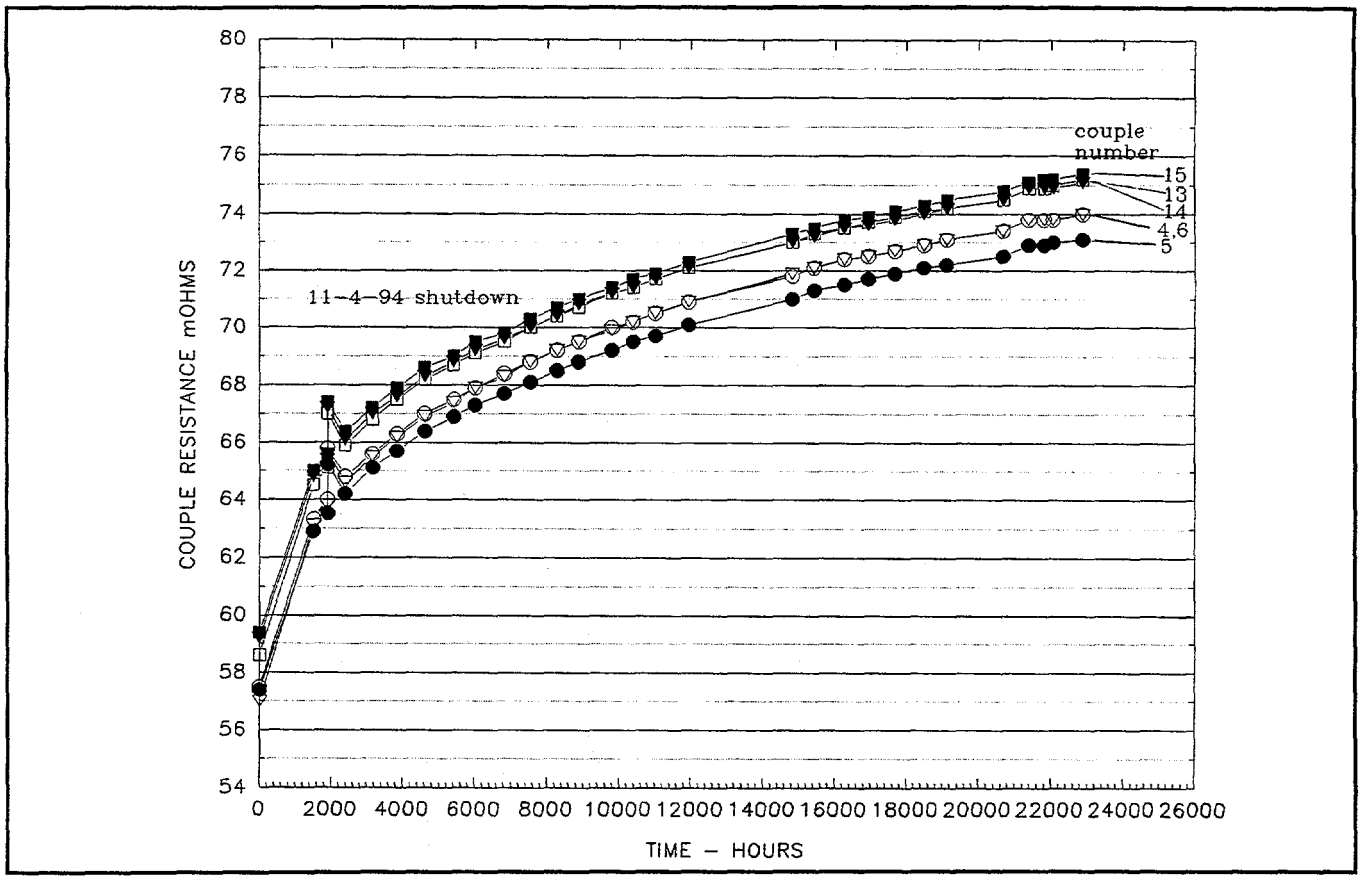

Figure 4-7. Individual Unicouple Internal Resistance Trends (Module 18-12)

Task 5

ETG Fabrication, Assembly, and Test

TASK 5 ETG FABRICATION, ASSEMBLY, AND TEST

Converter Hardware

All E-8 subassembly converter kits have been completed and placed in stock. Repackaging of residual unicouple and converter components for long term storage has also been completed. Repackaging of converter tooling for long term storage is in progress. Final editing of the videos depicting the unicouple and converter manufacturing processes is nearing completion and the unicouple production line continues to be maintained in a minimal shutdown mode.

Fabrication of replacement gas management hardware (fitting saver/flex hose assembly for the F-2, F-5, F-6, and F-7 RTGs has been completed. The hardware will be shipped to the Cape in April for subsequent change out by LMMS personnel. The PRDs for the F-2, F-5, F-6 and F-7 RTGs have been returned from Mound. They have successfully completed bellows force testing and leak testing. Final leak testing is scheduled for the end of May, after which they will be shipped to the Cape for installation in June.

Task 6

Ground Support Equipment (GSE)

TASK 6 GROUND SUPPORT EQUIPMENT (GSE)

GSE Hardware

Preparation of the GSE hardware in support of the Cape operations was the main activity this period. This included the inspection and minor rework of the shipping container bases and lifting yokes. The yokes and other handling fixtures were successfully proof loaded and dye penetrant inspected. Additionally, all calibrated equipment was re-calibrated prior to shipping to the Cape. The GSC manifolds were also fabricated, successfully leak tested and flow cleaned in preparation for Cape support operations. The first set of GSE hardware was shipped to the Cape in January and the second shipment will be in mid-April just prior to RTG arrival at the Cape.

Task 7

RTG Shipping and Launch Support

TASK 7 RTG SHIPPING AND LAUNCH SUPPORT

Launch Activity

LMMS personnel, at the request of JPL, have drafted RTG processing procedures for operations in the KSC RTG facility. In addition, LMMS personnel have reviewed and provided comments on draft procedures prepared by JPL.

LMMS personnel have also reviewed preliminary drawings of the ramps to be used to transfer the RTGs using the RTG Installation Cart from the top of the level 14 hatch to deck level.

Shipping Activity

LMMS personnel prepared draft procedures for the on-site transfers of the RTGs using the RTG transportation system trailers. The procedures were checked-out and refined during a walk through conducted at KSC in January. LMMS personnel also witnessed two walkthroughs of RTGTS package assembly and loading operations conducted by Mound personnel. Mound personnel also conducted unloading and loading walkthroughs at KSC and LMMS personnel participated in these activities as well.

Task 8

Designs, Reviews, and Mission Applications

TASK 8 DESIGNS, REVIEWS, AND MISSION APPLICATIONS

8.1 Galileo/Ulysses Flight Performance Analysis

No significant activity this reporting period.

8.2 Individual and Module Multicouple Testing

This task has been successfully completed.

8.3 Structural Characterization of Candidate Improved N- and P-Type SiGe Thermoelectric Materials

This task has been successfully completed.

8.4 Technical Conference Support

No significant activity this reporting period.

8.5 Evaluation of an Improved Performance Unicouple

Module 18-Z

This task has been successfully completed.

8.6 Solid Rivet Feasibility Study

This task has been successfully completed.

8.7 Computational Fluid Dynamics (CFD)

Work continues on the CFD task. Because this task is closely related to the Task 3 safety activities, technical progress is reported under that task.

8.8 Technical International Conference Support

This task has been successfully completed.

8.9 Additional Safety Tasks

Additional safety efforts have been assigned to this task. Because these efforts are closely related to the Task 3 safety activities, technical progress is being reported under that task.

8.10 SMALL RTG DESIGN STUDY

The small RTG conceptual design was presented to DOE in August of 1996, however, additional activity continued during this reporting period. Specifically, a compatibility study of the electric heat source insulator materials was planned, some materials were obtained, and fixtures were prepared.

The insulator materials selected for testing consist of Coors high purity alumina, which is similar to the present insulator material, and two types of silicon nitride. Samples of silicon nitride have been supplied by Morgan Matrock, Ltd., and Allied Signal, Inc. A fourth category of test specimen was alumina with a boron nitride coating. Kenntech was contacted but was unable to provide coating services at this time.

The test plan called for placing the various insulator materials in contact with Poco graphite on both faces, and measuring the isolation resistance as a function of temperature and time for periods of 200 to 2000 hours. Four fixtures were designed and fabricated for this purpose. Graphite and boron nitride parts for the test fixtures were machined, cleaned and baked-out in preparation for testing. However, these activities were suspended midway through the reporting period due to budget constraints.

Task 9

Project Management, Quality Assurance and Reliability, Contract Changes, Non-Capital CAGO Acquisition, and CAGO Maintenance

TASK 9 PROJECT MANAGEMENT, QUALITY ASSURANCE, AND RELIABILITY

9.1 Project Management

All weekly and monthly contractual reports were delivered on schedule.

During this period, LMMS supported the F-6 and F-7 RTG assembly and testing at Mound, including the government buy off meetings and the RTG Shipment Readiness Review meeting at Germantown, MD. All RTGs were approved for shipment.

All E-8 hardware is complete and in stock. Repackaging of the unicouple and converter hardware is complete. Repackaging of converter tooling is nearing completion.

It is planned to ship all GSE to the Cape on April 11 and begin LMMS launch site support operations immediately thereafter. All GSE hardware to be shipped to the Cape has completed annual calibration and/or proof load testing. Final C of I's are planned for early April prior to shipping date.

Attached is the Cassini RTG calendar showing 1Q97 and 2Q97 program meetings and important related events.

No significant environmental, health or safety incidents occurred during this period.

9.2 Quality Assurance

Quality Plans and Documents

No plans were initiated or modified during this period.

Process Readiness and Production Readiness Reviews

No readiness reviews were conducted this month.

Quality Control in Support of Fabrication

E-8 Converter Hardware: Quality Assurance support has been provided to support the fabrication of various sub-assemblies which are being completed for the E-8 converter and then placed into stock in the event that the converter is completed. Hardware completed during this period includes the shell and fin assembly, spare gas management valve assembly, RTD sensors, ceramic insulators and numerous fasteners and fittings. Where required, the hardware has been submitted for Certificate of Inspections and then placed in stock for future use.

Ground Support Equipment: In preparation for operations at the Cape, Ground Support Equipment such as shipping containers, lifting hardware and gas management hardware(flex hoses, etc.) have been inspected and presented for Certificates of Inspection, where required. This effort will continue, as required, to support the shipment date of 11 April 1997.

Material Review Board

There were no Class I (major) nonconformances generated this reporting period.

Quality Assurance Audits

There was no activity in this area during this reporting period.

Quality Assurance Status Meeting

There were no meetings held during this period.

Task H

Contract Acquired Government-Owned Property (CAGO) Acquisition

TASK H CONTRACTOR ACQUIRED GOVERNMENT OWNED (CAGO) PROPERTY ACQUISITION

Task H.1 CAGO Unicouple Equipment

No significant activity during this reporting period.

H.2 CAGO - ETG Equipment

No significant activity during this reporting period.

H.3 CAGO - MIS

No significant activity during this reporting period.

Program Calendars

Cassini RTG Program Calendar

As of 2 October 1996

3rd QTR 1996

	M	T	W	T	F	S	S	FW
JULY	1	2 DOE/HNUS Review of DFSAR - Valley Forge - *DeFillipo/Rutger/Firstenburg*	3	4	5	6	7	27
	8	9	10	11	12	13	14	28
	15	16	17	18	19	20	21	29
	22	23 Monthly Reports Due to DOE	24 Cassini Quarterly Program Review - OSC, Germantown, MD *Hemler, Cockfield, Reinstrom, DeFillipo*	25 F-2 Vibration Test - EG&G Mound - Miamisburg, OH- *Haley/Rosko/Kauffman/Rickenbach*	26	27	28	30
AUGUST	29	30	31	1	2	3	4	31
	5	6	7	8 GPHS EGA Reentry Event Tree Probabilities - JHU/APL - *DeFillipo/ Letts/ Hg/ Tobery / Kampas*	9	10	11	32
	12	13 RTG Data Package and P/FR Classification - EG&G Mound - *Reinstrom*	14	15	16	17	18	33
	19 F-7 Assembly Segment Readiness Review - EG&G Mound - *Reinstrom*	20	21	22	23 F-7 Assembly - EG&G Mound - Miamisburg, OH - *Cockfield* Monthly Reports Due to DOE	24	25	34
SEPTEMBER	26	27	28	29 Small RTG Design Review - OSC, Germantown - *Hemler, et al* Full Stack Intact Impact INSRP Briefing - JPL - Pasadena, CA *DeFillipo/ Rosko / Chan*	30	31	1	35
	2 **Labor Day** 	3 Rad Worker Training - EG&G Mound - *Haley/Dickinson* F-2 T/V Segment Readiness Review - EG&G Mound - *Kelly/Klee*	4 RTG Adapter Fit Check - EG&G Mound - *Haley/Dickinson* MET/BEES INSRP Meeting - LMMS San Jose -	5 F-7 Assembly Support - EG&G Mound - *Gosling* PSSP/LASP INSRP Meeting - LMMS Valley Forge -	6	7	8	36
	9	10	11	12	13	14	15	37
	16	17	18 Cassini Montly Program Review - OSC, Germantown, MD - *Hemler/ Reinstrom/ DeFillipo*	19 F-7 Assembly Support - EG&G Mound - Cockfield/Douglas	20	21	22	38
	23 Monthly Reports Due to DOE	24	25	26	27	28	29	39

Cassini RTG Program Calendar

As of 23 December 1996

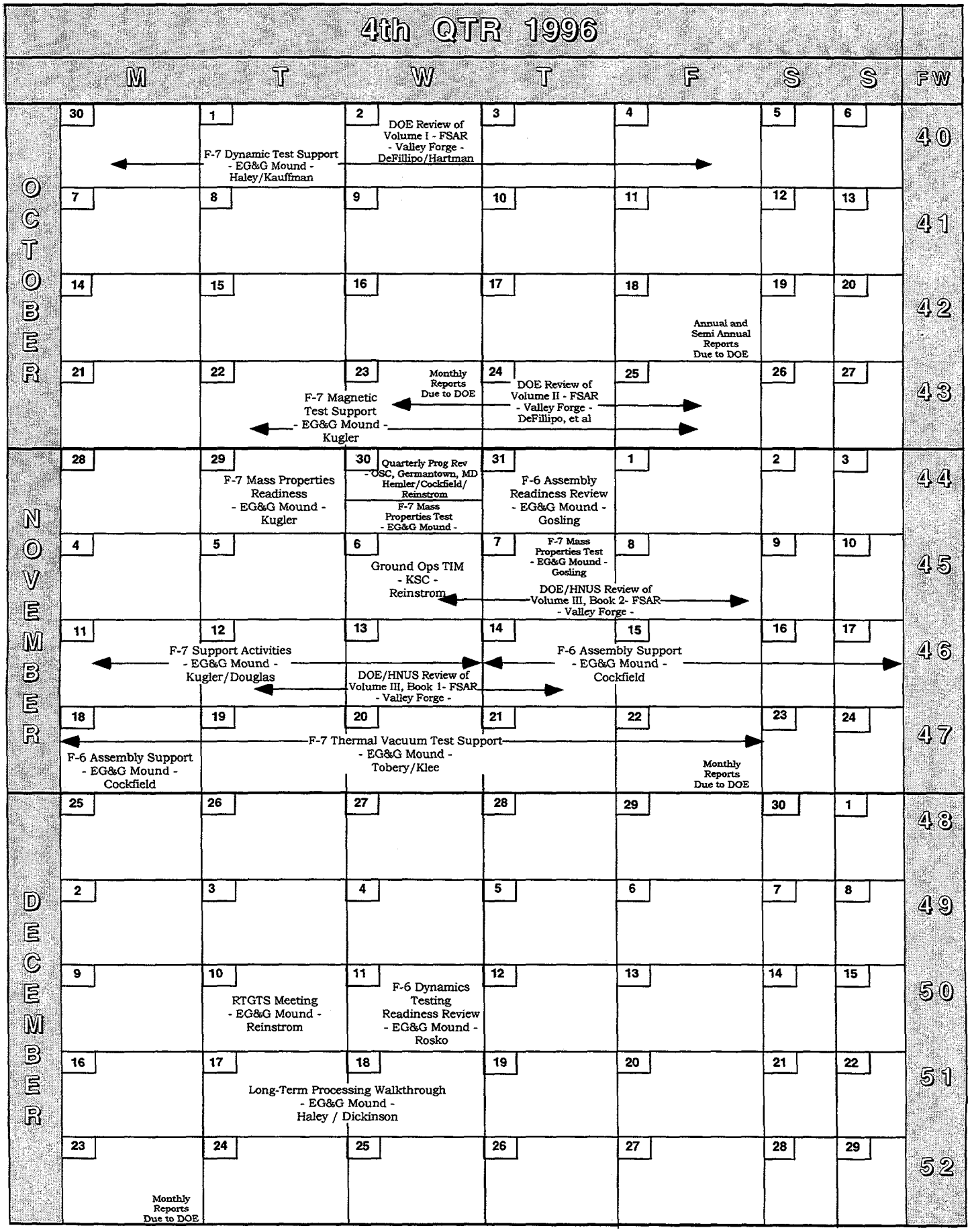

Cassini RTG Program Calendar

As of 26 March 1997

1st QTR 1997

	M	T	W	T	F	S	S	FW
JANUARY	30	31	1	2	3	4	5	01
	6	7 FSAR Vol III INSRP Information Exchange Meeting - San Jose - DeFillipo/Deane/Ha	8 RTG Tansportation System Walk-through - EG&G Mound - Haley/Reinstrom	9	10	11	12	02
	13	14 Magnetics Testing - EG&G Mound - Kugler	15	16 RTG Tansportation System Walk-through - Kennedy Space Center - Florida - Haley/Reinstrom	17	18	19	03
	20	21	22	23 Monthly Reports Due to DOE	24	25	26	04
FEBRUARY	27	28 F-6 Mass Properties Test Support - Mound - Gosling/Grimley	29	30	31	1	2	05
	3	4 Space Technology & Applications International Forum (STAIF-97) - Albuquerque, New Mexico - Hemler/Cockfield/Josloff	5 INSRP Meeting on FSAR Addendum - Valley Forge Sheraton - DeFillipo, et al.	6 INSRP Meeting on FSAR Interchange - Valley Forge Sheraton - DeFillipo,et al.	7 F-6 Thermal Vacuum Test - EG&G Mound - Kelly	8	9	06
	10	11	12	13	14	15	16	07
	17	18	19 Quarterly Review - EG&G Mound - Hemler/Reinstrom/ Cockfield/DeFillipo	20 F-2, F-7 Buy -Off - EG&G Mound - Reinstrom/Cockfield	21 Monthly Reports Due to DOE	22	23	08
MARCH	24	25	26	27	28	1	2	09
	3	4	5	6	7	8	9	10
	10	11 RTG TS Walkthrough - EG&G Mound - Reinstrom/Haley	12	13	14	15	16	11
	17	18 INSRP Reentry Meeting - Los Angeles - Hemler/DeFillipo/ Tobery/Daywitt/Vacek	19	20	21 Monthly Reports Due to DOE	22	23	12
	24	25	26 F-6 Buy-Off Review - DOE-HQ Germantown - Reinstrom/Cockfield	27 Shipment Readiness Review - DOE-HQ Germantown - Hemler/Reinstrom Haley/Cockfield	28	29	30	13

Cassini RTG Program Calendar

As of 9 April 1997

2nd QTR 1997

	M	T	W	T	F	S	S	FW
APRIL	31	1	2	3	4	5	6	14
		Capacitance Testing - EG&G - Mound - Haley						
	7	8	9	10	11	12	13	15
	Shipment Preps & Training - EG&G - Mound - Reinstrom							
	14	15	16	17	18	19	20	16
	Cassini Launch Team Leaves for Cape Canaveral Haley/Dickinson/Fry/ Douglas/Chermak				Semi Annual Reports Due to DOE			
				RTG Shipment Review & Preparation - EG&G - Mound - Reinstrom				
	21	22	23	24	25	26	27	17
			Monthly Reports Due to DOE					
MAY	28	29	30	1	2	3	4	18
	5	6	7	8	9	10	11	19
	12	13	14	15	16	17	18	20
	19	20	21	22	23	24	25	21
					Monthly Reports Due to DOE			
JUNE	26	27	28	29	30	31	1	22
	2	3	4	5	6	7	8	23
	9	10	11	12	13	14	15	24
	16	17	18	19	20	21	22	25
	23	24	25	26	27	28	29	26
	Monthly Reports Due to DOE							